PWR and BWR Spent Fuel Assembly Gamma Spectra Measurements

S. Vaccaro[a], S.J. Tobin[b], A. Favalli[b], B. Grogan[c], P. Jansson[d], H. Liljenfeldt[1c], V. Mozin[f], J. Hu[c], P. Schwalbach[a], A. Sjöland[e], H. Trellue[b], D. Vo[b]

[a]European Commission, DG Energy, Directorate EURATOM Safeguards Luxembourg (Luxembourg); [b]Los Alamos National Laboratory, Los Alamos NM (USA); [c]Oak Ridge National Laboratory, Oak Ridge (USA); [d]Uppsala University, Uppsala (Sweden); [e]Swedish Nuclear Fuel and Waste Management Company (SKB) (Sweden); [f]Lawrence Livermore National Laboratory, Livermore CA (USA)

Abstract

A project to research the application of nondestructive assay (NDA) to spent fuel assemblies is underway. The research team comprises the European Atomic Energy Community (EURATOM), embodied by the European Commission, DG Energy, Directorate EURATOM Safeguards; the Swedish Nuclear Fuel and Waste Management Company (SKB); two universities; and several United States national laboratories. The Next Generation of Safeguards Initiative – Spent Fuel project team is working to achieve the following technical goals more easily and efficiently than in the past using nondestructive assay measurements of spent fuel assemblies: (1) verify the initial enrichment, burnup, and cooling time of facility declaration; (2) detect the diversion or replacement of pins, (3) estimate the plutonium mass, (4) estimate the decay heat, and (5) determine the reactivity of spent fuel assemblies. This study focuses on spectrally resolved gamma-ray measurements performed on a diverse set of 50 assemblies [25 pressurized water reactor (PWR) assemblies and 25 boiling water reactor (BWR) assemblies]; these same 50 assemblies will be measured with neutron-based NDA instruments and a full-length calorimeter. Given that encapsulation/repository and dry storage safeguards are the primarily intended applications, the analysis focused on the dominant gamma-ray lines of ^{137}Cs, ^{154}Eu, and ^{134}Cs because these isotopes will be the primary gamma-ray emitters during the time frames of interest to these applications. This study addresses the impact on the measured passive gamma-ray signals due to the following factors: burnup, initial enrichment, cooling time, assembly type (eight different PWR and six different BWR fuel designs),

[1] Formerly Swedish Nuclear Fuel and Waste Management Company (SKB)

presence of gadolinium rods, and anomalies in operating history. To compare the measured results with theory, a limited number of ORIGEN-ARP simulations were performed.

Keywords: Passive Gamma;, Burnup; Cooling time; Gamma spectroscopy; Spent Fuel; Nuclear Safeguards; Germanium Detector; Final Disposal; Non-destructive Assay.

1. Introduction

A project to research the application of nondestructive assay (NDA) to spent fuel assemblies is underway at the central interim storage facility for spent nuclear fuel (Clab) in Oskarshamn, Sweden. The project is a collaboration among the European Atomic Energy Community (EURATOM), embodied by the European Commission, DG Energy, Directorate EURATOM Safeguards; the Swedish Nuclear Fuel and Waste Management Company (SKB); two universities; and several United States (US) national laboratories (Los Alamos National Laboratory, Oak Ridge National Laboratory, Lawrence Livermore National Laboratory) participating in the Next Generation Safeguards Initiative–Spent Fuel (NGSI–SF) project [1][2].The research goals of this project contain both safeguards and non-safeguards interests. The safeguards interest include (1) verifying that a given assembly is the assembly that the facility has declared to the regulators [International Atomic Energy Agency (IAEA), EURATOM, and national authorities], which involves confirming the initial enrichment, burnup, and cooling time of each assembly; and (2) verifying that the integrity of a spent fuel assembly is maintained by detecting missing or replaced fuel pins. In addition, the interests of the Swedish facility and/or domestic regulations motivate the inclusion of the following technical goals: (3) rapidly estimating the heat content in each individual assembly and (4) measuring the reactivity of each assembly to ensure that all potential fuel configurations are safe in terms of heat and criticality.

This study focuses on the passive gamma measurements made at Clab using SKB's in-pool passive gamma measurement station. These measurements were made during four campaigns that took place

between August 2013 and December 2014. The NDA research needs and/or lessons learned from (1) the Central Storage of Spent Nuclear Fuel and Encapsulation Plant, (2) the safeguard inspectorates [IAEA, EURATOM, and the Swedish Radiation Safety Authority, (SSM)], and (3) the NGSI-SF project have combined to shape both the fuel selection and measurement settings of this project. The 50 fuel assemblies selected for measurement (see Tables 1 and 2) were chosen to span a wide range of fuel parameters, such as fuel type, initial enrichment, and burnup, that are anticipated to be representative of the fuels to be disposed of in the Swedish repository. The eventual NDA system selected for the Clink facility (the encapsulation plant which is going to be integrated with the Clab facility), must be capable of handling this kind of diversity. With respect to the cooling time of the fuel, it is expected that the Clink facility will accept only fuel that has cooled between 10 and ~60 years. This selected time interval motivated a focus on gamma spectral lines detectable during that time interval, in particular ^{137}Cs and ^{154}Eu, but not to exclude the lines from shorter-lived gamma-ray emitters such as ^{134}Cs. The selection of this cooling-time range is relevant to the safeguards inspection need for "more sensitive and less intrusive alternatives to existing nondestructive assay instruments to perform partial defect tests on spent fuel assemblies prior to transfer to difficult to access storage" described in the IAEA's Department of Safeguards Long-Term R&D Plan [3]. This verification need, which includes dry storage, as well as encapsulation applications, increased the interest in assemblies with cooling times of ~5 years.

An additional influence on both the fuel selection and measurement settings is the lessons learned over the duration of the NGSI-SF project. At the most general level, the NGSI-SF project seeks to quantify the capabilities and limitations of several integrated NDA systems to characterize spent fuel assemblies for safeguards purposes. However, in pursuit of the technical goals described earlier, the use of data mining analysis techniques is planned to obtain useful quantitative patterns among the measured signatures. The primary motivation for using data mining techniques to look for patterns is the isotopic complexity of spent fuel, both in terms of what isotopes are formed in a reactor and how these isotopes vary as a function of time once they leave the reactor [5]. To determine what useful patterns may exist among the

77 data, it was necessary to create a database of NDA signatures. The research presented here describes the
78 passive gamma data input to this database.

79 ## 2. Experimental Setup

80 ### 2.1. Description of assemblies in the SKB-50

81 To test the gamma-ray detectors and the advanced NDA instruments developed under the NGSI-SF
82 project, 50 spent fuel assemblies from Clab were selected (Tables 1 and 2) for measurements. Of these 50
83 assemblies, known as the SKB-50, 25 PWR assemblies were selected with initial ^{235}U enrichment values
84 that span from 2.1% to 4.1%, burnup values that span from 20 to 53 GWd/tU, and cooling-time values
85 that span from 4 to 30 years; 20 of the PWR assemblies are 17 × 17, whereas 5 are 15 × 15. Of the 25
86 boiling-water-reactor (BWR) assemblies selected, initial enrichment spans from 1.3% to 3.4%, burnup
87 spans from 9 to 46 GWd/tU and cooling time spans from 7 to 27 years. For the 25 PWR assemblies, 8
88 different fuel designs are included, whereas for the BWR assemblies, 6 different fuel designs are
89 included; thus, some geometric variations exist among both fuel types.

90

Table 1. Fuel characteristics for the SKB-50 PWR assemblies. The cooling time is the time between discharge and the time of measurement for which the October 2014 measurement dates were used.

Assembly ID	Fuel Type	Initial Enrichment (^{235}U%)	Burnup (GWd/tU)	Cooling Time (yrs)	Loading (L)	Discharge (D)	Time D-L (yrs)
PWR1	15×15 PWR Fuel Type 1	4.096	52.6	5.4	04/05/2005	28/05/2009	4.07
PWR2	15×15 PWR Fuel Type 1	3.925	49.6	5.4	04/05/2005	29/05/2009	4.07
PWR3	17×17 PWR Fuel Type 1	3.694	48.2	14.3	06/07/1996	21/06/2000	3.96
PWR4	17×17 PWR Fuel Type 2	3.934	46.9	6.3	26/09/2004	04/06/2008	3.69
PWR5	17×17 PWR Fuel Type 2	3.937	46.9	6.4	26/09/2004	02/06/2008	3.68
PWR6	17×17 PWR Fuel Type 3	3.600	45.7	15.3	08/07/1993	23/06/1999	5.96
PWR7	17×17 PWR Fuel Type 4	3.944	44.5	7.3	05/09/2003	27/06/2007	3.81
PWR8	17×17 PWR Fuel Type 5	3.306	44.4	26.1	20/08/1984	11/09/1988	4.06
PWR9	15×15 PWR Fuel Type 2	3.701	45.8	7.2	15/06/2003	01/08/2007	4.13
PWR10	17×17 PWR Fuel Type 1	3.697	43.5	16.3	01/07/1994	17/06/1998	3.96
PWR11	17×17 PWR Fuel Type 1	3.505	43.2	14.3	01/07/1994	21/06/2000	5.97
PWR12	17×17 PWR Fuel Type 5	3.299	43.0	26.1	20/08/1984	11/09/1988	4.06
PWR13	15×15 PWR Fuel Type 3	3.199	40.9	27.5	25/07/1982	25/04/1987	4.75
PWR14	17×17 PWR Fuel Type 1	3.505	40.7	17.3	08/07/1993	24/06/1997	3.96
PWR15	17×17 PWR Fuel Type 5	2.803	40.5	27.1	17/04/1982	27/08/1987	5.36
PWR16	17×17 PWR Fuel Type 1	3.601	40.4	18.3	23/06/1993	21/06/1996	3.00
PWR17	17×17 PWR Fuel Type 1	3.704	40.3	15.1	22/09/1994	01/09/1999	4.94
PWR18	17×17 PWR Fuel Type 1	3.426	39.8	19.3	09/07/1989	09/06/1995	5.92
PWR19	15×15 PWR Fuel Type 4	3.185	35.0	29.4	17/05/1980	01/05/1985	4.96
PWR20	17×17 PWR Fuel Type 5	3.101	34.0	28.3	04/07/1980	18/06/1986	5.95
PWR21	17×17 PWR Fuel Type 5	3.101	34.0	28.3	04/07/1980	18/06/1986	5.95
PWR22	17×17 PWR Fuel Type 5	2.801	31.2	28.2	18/04/1982	10/08/1986	4.31
PWR23	17×17 PWR Fuel Type 1	3.502	28.5	18.3	07/07/1993	21/06/1996	2.96
PWR24	17×17 PWR Fuel Type 5	2.109	23.2	19.3	02/07/1980	09/06/1995	14.93
PWR25	17×17 PWR Fuel Type 5	2.110	19.6	30.4	03/07/1980	24/05/1984	3.89

Table 2. Fuel characteristics for the SKB-50 BWR assemblies set. The cooling time is the time between discharge and the time of measurement for which the December 2014 dates were used.

Assembly ID	Fuel Type	Initial Enrichment (235U%)	Burnup (GWd/tU)	Cooling Time (yrs)	Loading (L)	Discharge (D)	Time D-L (yrs)
BWR1	10×10 BWR Fuel Type 1	3.144	46.4	8.3	28-Oct-1999	29-Aug-2006	6.8
BWR2	10×10 BWR Fuel Type 2	3.204	43.8	10.3	9-Jun-1999	17-Aug-2004	5.2
BWR3	10×10 BWR Fuel Type 2	3.413	43.6	12.3	18-Aug-1996	12-Aug-2002	6.0
BWR4	10×10 BWR Fuel Type 2	3.415	43.0	12.3	18-Aug-1996	12-Aug-2002	6.0
BWR5	10×10 BWR Fuel Type 1	3.146	42.0	8.3	28-Oct-1999	29-Aug-2006	6.8
BWR6	8×8 BWR Fuel Type 1	2.680	41.4	29.2	5-Aug-1978	12-Sep-1985	7.1
BWR7	10×10 BWR Fuel Type 2	3.154	41.2	10.3	9-Jun-1999	17-Aug-2004	5.2
BWR8	10×10 BWR Fuel Type 3	3.147	39.7	9.5	29-Aug-2001	19-May-2005	3.7
BWR9	10×10 BWR Fuel Type 1	3.145	40.4	7.2	29-Aug-2001	7-Sep-2007	6.0
BWR10	10×10 BWR Fuel Type 1	3.144	39.5	8.3	29-Aug-2001	29-Aug-2006	5.0
BWR11	8×8 BWR Fuel Type 1	2.325	38.8	22.3	8-Nov-1980	22-Aug-1992	11.8
BWR12	10×10 BWR Fuel Type 4	2.962	33.5	9.5	24-Jun-1997	10-Jun-2005	8.0
BWR13	10×10 BWR Fuel Type 4	2.962	36.8	9.5	24-Jun-1997	10-Jun-2005	8.0
BWR14	8×8 BWR Fuel Type 1	2.637	36.1	29.2	5-Aug-1978	12-Sep-1985	7.1
BWR15	8×8 BWR Fuel Type 1	2.320	35.9	25.3	5-Nov-1980	25-Aug-1989	8.8
BWR16	8×8 BWR Fuel Type 1	2.323	35.8	27.5	5-Nov-1980	11-Jun-1987	6.6
BWR17	8×8 BWR Fuel Type 1	2.779	32.7	28.4	1-Mar-1975	15-Jul-1986	11.4
BWR18	8×8 BWR Fuel Type 1	2.096	31.9	22.3	14-Nov-1980	22-Aug-1992	11.8
BWR19	8×8 BWR Fuel Type 1	2.581	30.8	25.5	17-Oct-1984	10-Jun-1989	4.6
BWR20	10×10 BWR Fuel Type 4	2.975	26.4	9.5	2-Aug-1998	10-Jun-2005	6.9
BWR21	8×8 BWR Fuel Type 1	2.779	27.7	27.4	1-Mar-1975	1-Jul-1987	12.3
BWR22	10×10 BWR Fuel Type 4	2.975	20.4	9.5	14-Jul-2001	10-Jun-2005	3.9
BWR23	10×10 BWR Fuel Type 4	2.975	16.0	9.5	24-May-1999	10-Jun-2005	6.0
BWR24	8×8 BWR Fuel Type 2	1.281	13.3	27.4	17-Oct-1984	10-Jul-1987	2.7
BWR25	8×8 BWR Fuel Type 2	1.284	9.1	27.4	17-Oct-1984	10-Jul-1987	2.7

99 The fuel selected for the SKB-50, particularly among the BWR assemblies, is somewhat atypical of the
100 fuel used in Sweden in terms of operating histories. The selection process for assemblies was influenced
101 by the practical need to minimize the number of large multiple-assembly storage containers moved from
102 the lower pools at Clab to the upper pools. Thus, containers full of assemblies of the same basic
103 parameters, which were the most common case, were not selected; instead, containers with several unique
104 assemblies were selected. The end result is that the fuel in the SKB-50 is more variable in terms of reactor
105 operation history as compared with a more random selection process. More specifically, ~30% of the
106 selected assemblies experience at least 1 cycle out of the reactor between the first and last cycles in the
107 reactor; 16 BWRs and 6 PWRs experience more than 5.9 years between first entering the reactor and
108 finally leaving it, a fact tabulated as "Time D-L" in Tables 1 and 2. Additionally, two PWRs and seven
109 BWRs came from startup cores, which had lower initial enrichments and lower burnups. All BWR
110 assemblies have burnable poisons, whereas seven PWRs have burnable poisons: this fact is not an
111 anomaly because the most recent fuel designs tend to use more and more burnable poisons to improve
112 reactor operations. Finally, one BWR assembly contains part-length rods; thus, the number of actual rods
113 at the top of the assembly is fewer compared with the middle and the bottom.

114 **2.2. Physical setup and general operations**

115 The experimental setup was designed into Clab (see Figure 1). On the wall of the pool, a collimator slit,
116 ~10 m below the surface level of the water, allows a collimated gamma-ray beam into a neighboring room
117 where different detectors and acquisition systems were installed. The setup included a pool-based
118 mechanical system that can move the fuel assembly vertically and also rotate it around its central axis.
119 The horizontal width of the collimator allowed the entire horizontal extent of the assembly to be viewed.
120 The vertical width of the collimator's slit was set as 5 mm for all measurements. This vertical collimator
121 width corresponds to a 15-mm projection onto the assembly. The distance between the center of the
122 assembly and the pool wall is ~0.5 m, and the distance from the center of the assembly to the end of the

collimator is 2.46 m, [6] [8]. Although not used, the collimator can be rotated as well as reduced to 1 or 2 mm in slit width.

For this collimator setup, measurements were made with the assembly in a fixed position, as well as with the assembly moving past the collimator vertically. For the spectra obtained while the fuel moved, or scanned, past the collimator, the count time was set by the time needed to move the fuel both up and down; thus, the full length of the assembly was scanned twice. Note that one single spectrum was collected with the Pulse Height Analysis (PHA) data acquisition system when the fuel was moving; thus, the intensity of all lines is an average over the assembly. With the list-mode system, by which every pulse is time-stamped, it is possible to look at the axial section of the fuel in post-processing. The combined time needed for the fuel to go up and down was ~402 s for PWR assemblies, 400 s for non-slowly varying-envelope-approximation (SVEA)-type BWR assemblies, and 406 s for SVEA-type BWR assemblies. This time was determined with the list mode system by noting when 662-keV photons from ^{137}Cs were detected in front of the collimator. The current study is based on the data from static measurements. A separate publication dedicated to the analysis of the data obtained with the list mode system while the fuel moved vertically is to be submitted [9].

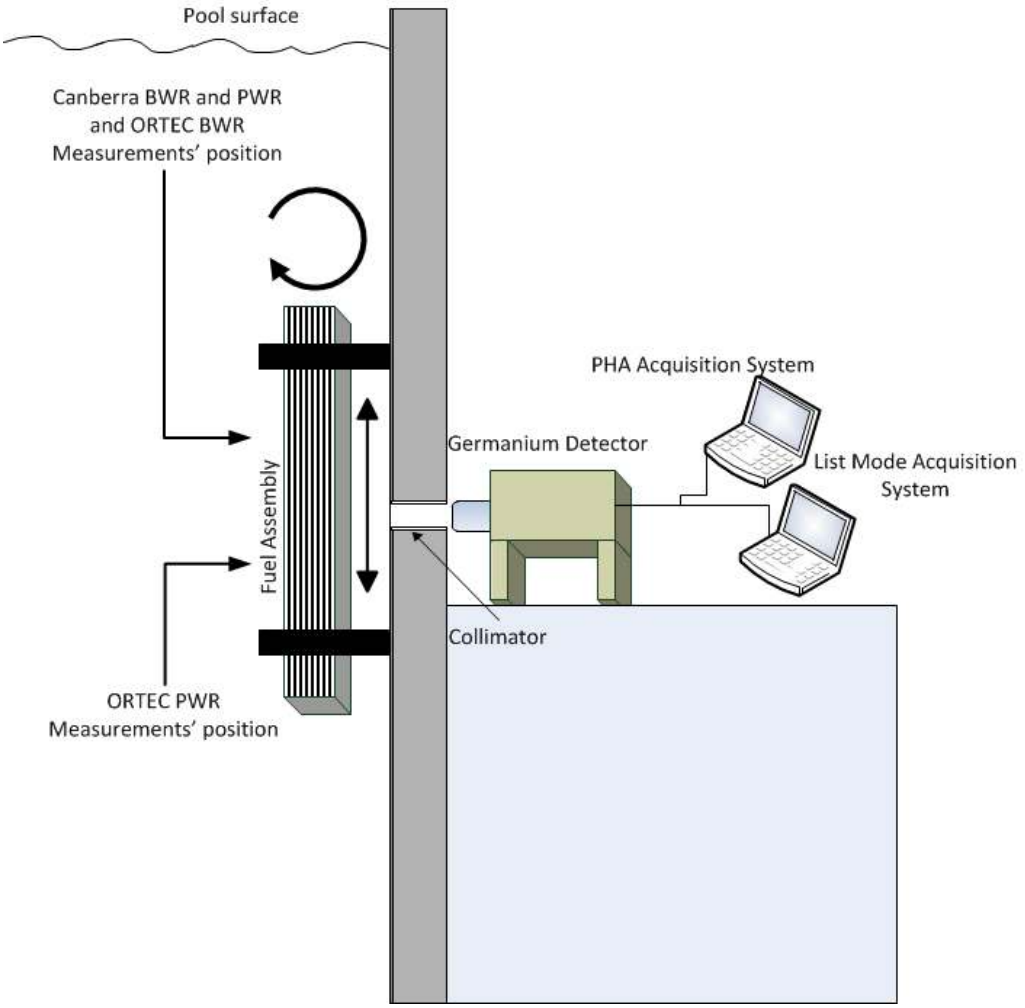

Figure 1. Scheme of the measurement setup in which PHA stands for pulse height analyzer.

The passive gamma spectra were measured in four different measurement campaigns in 2013 and 2014 at Clab. Two different p-type coaxial high-purity germanium (HPGe) detectors were used. In all campaigns, when the assembly was moved in front of the collimator during data collection, the signal from the HPGe detector was branched to two multichannel analyzers (MCAs). During the first two campaigns, Lawrence Livermore National Laboratory provided an ORTEC GMX detector and a Canberra Lynx MCA [26] to acquire the PHA spectra; SKB provided a Canberra Lynx MCA to collect the list mode data. During the latter two measurement campaigns, EURATOM provided a Canberra GX detector and a digital MCA-527 by GBS Elektronik [10] to collect the PHA data; SKB provided a Canberra Lynx MCA to collect the list mode data. Another Lynx MCA was provided by Los Alamos National Laboratory for medium-resolution

measurements with a $LaBr_3$ detector, beyond the scope of the present paper. Because of the different detector characteristics and a desire to operate at a higher count rate during the latter two campaigns, different thicknesses of absorber sheets were placed between the detector crystal and the collimator among the campaigns (see Table 3, detectors characteristic are reported as taken from data sheets of the producers [10, 26]).

For the fixed axial location measurements, mostly only the MCAs set to PHA mode were used. When measuring a fixed axial location, in most cases, just the PHA data acquisition was performed. This decision was made as the benefits inherent in list mode, such as post processing capability, were counter balanced with the necessity of storing and managing large files. For a static measurements, the likely benefit from list mode was considered not significant. Between the first two measurements campaigns at Clab and the last two campaigns, a new support structure for the HPGe detector was fabricated by Clab. This structure allowed the detector to be easily moved vertically in front of the collimator. This feature helped to determine the location for obtaining optimal vertical detector position with respect to the collimator slit, corresponding to the maximum count rate and optimum signal-to-background ratio. The end position had the central axis of the detector crystal 3 mm below the vertical plane of the collimator.

Table 3. Comparison between the two detector setups used

	Campaign 1 and 2	**Campaign 3**	**Campaign 4**
Detector type	ORTEC GMX (Coaxial HPGe)	Canberra GX (Coaxial HPGe)	Same as campaign 3
Relative efficiency at 1.33 MeV	44%	44%	
Resolution at 1.33 MeV (FWHM keV)	2.0	1.8	
Peak-to-Compton ratio	60:1	69:1	
Trapezoidal rise time	3 μs	3 μs	
Trapezoidal flat top	0.6 μs	1 μs	
Absorbers positioned between detector crystal and collimator	– 8 mm lead – 12 mm stainless steel – 1 mm copper	– 8 mm lead – 21 mm stainless steel – 3 mm aluminum – 1 mm copper	– 3.2 mm lead – no stainless steel – no aluminum – 1 mm copper

[a]FWHM = Full width half-maximum.

In nearly all cases in the last 2 campaigns, 8 spectra were measured for each of the 50 assemblies: 1 axial up-and-down scan for each of the 4 corners and 1 static measurement on the burnup plateau for each corner. Given that only two isotopes emit a reasonable amount of detectable photons over the duration of interest to the Clink facility, ^{137}Cs and ^{154}Eu, due to half-lives of 30.1 years and 8.59 years, respectively, the net peak areas, in counts per second (cps), from these two isotopes are of primary interest. Because the 662-keV line of ^{137}Cs line is so dominant, the statistical uncertainty of the peak areas was always <1%. Thus, the guiding metric for count time selection was the detection of the most dominant line of ^{154}Eu, the 1274-keV line, to <~1% statistical uncertainty for the average count rate among the assembly's corners.

The experimental plan for the measurement of spectral lines was to measure in a way that weighted a photon from each of the outer pins in a nearly identical manner. We decided to point each corner of the assemblies toward the collimator for 4 different measurements for two primary reasons: (1) When the spectra from all the corners are added together, each exterior pin is nearly weighted the same. Simulations [8] indicate that a pin on the center of a face is weighted at ~80% of the corner pin on a per photon basis for a 662 keV photon. (2) The spectral intensity is insensitive to assembly rotation within the possible range of motion when the corner is pointed toward the collimator; the same is not true when a flat side of the assembly is pointed toward the collimator. All results in this paper, except where notes otherwise, used data that was averaged over all 4 corners. The reason why one corner only was measured in the first two campaigns was because it was not possible to measure the other corners, due to mechanical difficulties. However, this restriction provided time to measure more axial locations and to have longer measurement times. Furthermore, two independent detectors measured one corner of a significant fraction of the SKB-50 assemblies, which allowed for comparison between the systems, providing confidence in the quality of the data. The assembly positions measured in the first two campaigns were re-measured in the latter two campaigns and as such are not a part of the data illustrated in the paper, except where noted otherwise.

3. Experimental Results

3.1. General features of the acquired spectra

Figures 2 and 3 present some examples of the acquired spectra for BWR and PWR assemblies with features spanning over the range of the available fuel. The main peaks, which will be analyzed in the following paragraphs, are marked.

As a qualitative analysis, we can observe that shorter lived isotopes, as ^{134}Cs, are not detectable in the older fuel and cannot be taken into account for those assemblies characterization who require quantitative evaluation of their peak area (i.e. for burnup or cooling time calculation).

Even if shorter cooled fuel exhibits a high dead time (above 40% both for BWR and PWR fuel), the consequent resolution degradation is still tolerable: in fact we can still observe a clear separation between the two peaks of the 996 keV – 1004 keV doublet from ^{154}Eu. The set-up conditions are thus proving to be compatible with an acceptable detector performance even at a high count rate.

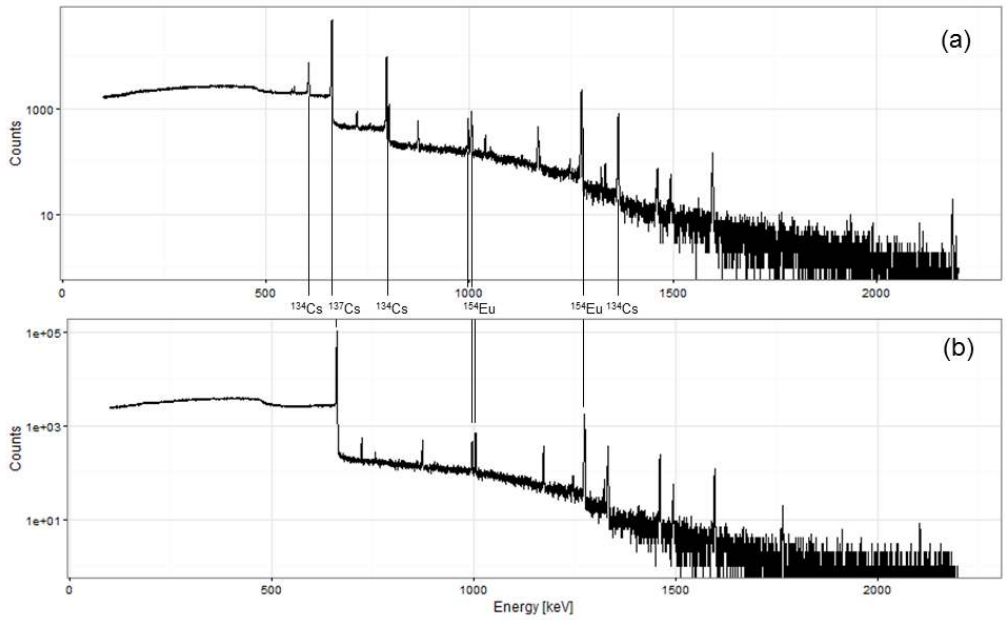

Figure 2. Gamma Spectra from BWR irradiated fuel assemblies. (a) BWR9: 7.2 years cooling time, 43.10% deadtime, 100s livetime ; (b) BWR 6: 29.2 years cooling time and 18.03% deadtime, 400s livetime.

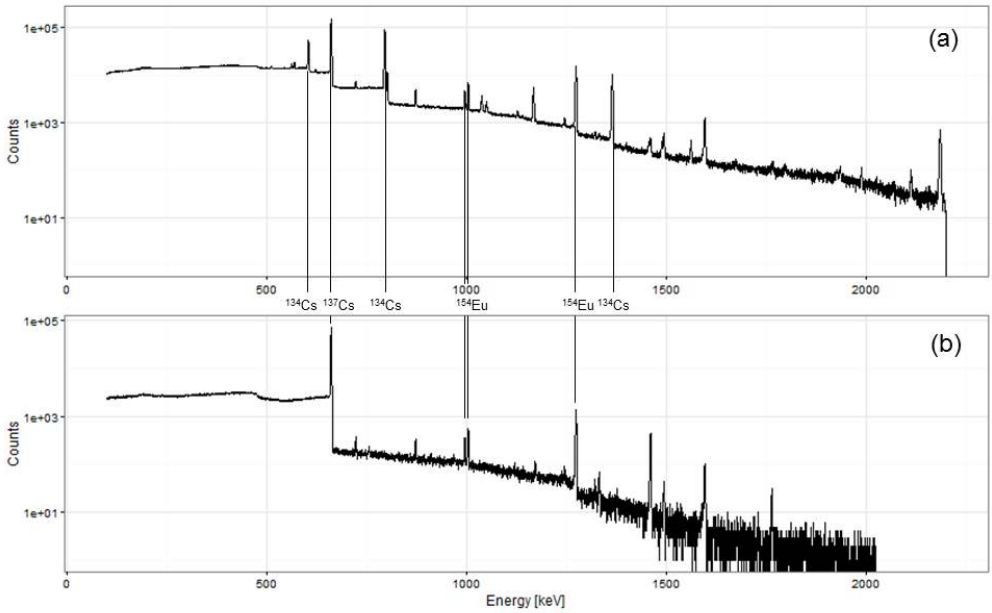

Figure 3. Gamma Spectra from PWR irradiated fuel assemblies. (a) PWR4: 5.2 years cooling time, 44.45% deadtime, 515s livetime ; (b) PWR25: 30.4 cooling time and 5.97% deadtime, 872.9s livetime.

3.2. Spectra evaluation method

The spectra were analyzed in two ways. The isotopic analysis code Fixed energy Response function Analysis with Multiple efficiencies (FRAM) was used [11], [12]. The basic function of FRAM fits various regions of the spectrum to obtain the areas of the peaks, and from these the code calculates the total efficiencies of the photon peaks that are detected. This total efficiency includes detector efficiency, geometry, sample self-absorption, and attenuation in materials between the sample and the detector. It then calculates the relative activities of the isotopes using the ratio technique. However, for the current paper, only the net peak areas were used, whereas other papers by NGSI-SF researchers will deal with a detailed analysis of the FRAM spectra evaluation and isotope ratios [13], [14], [15]. Additionally, for the spectra obtained with the ORTEC GMX, the net peak areas were determined using the Genie 2000 software [16] connected to the Lynx electronics, whereas for the data taken with the Canberra GX detector, an additional analysis of the net peak area was done using the PeakEasy software [17]. For the

static measurements, the spectra were dead-time corrected, using the value of dead-time reported respectively by the Lynx electronics, for the data taken with the ORTEC GMX detector, or estimated by the MCA-527 electronics [18] for the other campaigns.

In Table 4, for the PHA data obtained from the burnup plateau, the average count rate among the four corners' static measurements is listed for each peak. The 1-sigma statistical uncertainty, as reported, in the average count rate was calculated by taking the square root of the sum of the square of each individual measurement. For most peaks of most assemblies, this statistical uncertainty is smaller than the variation in the photon flux from the different corners of the assembly, which is caused primarily by variation in the fuel burnup of each corner.

For the geometric setup used, the gamma rays generated in the fuel rods closer to the collimator have larger contribution to the gamma-ray flux density of the full-energy peak than the gamma rays originating from other rods. Indeed, the detection probability of emitted photons of depends both on their energy and on the pin from they originate. As shown by the Monte Carlo calculations by Jansson et al. [8] in Figure 4, self-absorption of photons within the assembly is a very large factor, resulting in roughly 90% of the detected photons coming from the outer two rows for all energies.

248

249 **Table 4. Net Peak intensities measured for the most prominent gamma-ray-emitting isotopes from the**
250 **assemblies in the SKB-50. The data were obtained with the Canberra GX detector and GBS Elektroniks'**
251 **MCA-527, and the net peak areas are the average of all four corners' static measurements. No correction was**
252 **made for decay time because discharge was applied to the data. (ND = Nondetectable; NA = Nonapplicable)**

	137-Cs	*Unc.*	*154-Eu*	*Unc.*	*154-Eu*	*Unc.*	*154-Eu*	*Unc.*	*134-Cs*	*Unc.*	*134-Cs*	*Unc.*
	662 keV		**996 keV**		**1004 keV**		**1274 keV**		**605 keV**		**796 keV**	
	(cts/s)	**(%)**	**(cts/s)**	**(%)**	**(cts/s)**	**(%)**	**(cts/s)**	**(%)**	**(cts/s)**	**(%)**	**(cts/s)**	**(%)**
PWR1	1780	0.26%	41.84	1.61%	73.84	1.01%	259.6	0.52%	516.2	0.39%	1253.	0.36%
PWR2	1693	0.28%	38.71	1.47%	69.06	0.98%	241.1	0.55%	439.0	0.49%	1059.	0.40%
PWR3	1339	0.32%	18.05	1.45%	32.19	1.00%	114.2	0.77%	22.49	2.12%	56.94	0.67%
PWR4	1397	0.27%	30.19	1.56%	55.14	1.00%	194.3	0.61%	245.0	0.51%	603.2	0.36%
PWR5	1364	0.27%	29.75	1.49%	52.24	0.99%	188.4	0.61%	238.1	0.54%	583.3	0.33%
PWR6	1217	0.35%	15.36	1.34%	27.32	0.96%	99.19	0.72%	13.86	2.95%	33.93	0.83%
PWR7	1354	0.30%	26.51	1.54%	48.01	0.99%	172.9	0.62%	173.2	0.65%	415.7	0.48%
PWR8	946	0.37%	6.08	1.63%	11.14	1.10%	40.07	0.77%	ND	NA	0.86	8.47%
PWR9	1505	0.30%	28.81	1.51%	51.28	0.99%	185.8	0.61%	205.2	0.55%	497.0	0.44%
PWR10	1176	0.35%	13.18	1.74%	23.52	1.16%	84.61	0.88%	9.28	4.31%	21.68	1.15%
PWR11	1133	0.40%	14.65	1.51%	25.66	1.00%	91.03	0.87%	11.31	3.58%	27.06	1.00%
PWR12	962	0.38%	5.94	1.63%	10.51	1.11%	37.76	0.81%	ND	NA	1.04	7.07%
PWR13	812	0.33%	4.52	1.46%	8.03	0.96%	29.00	0.81%	ND	NA	0.51	9.77%
PWR14	1055	0.39%	11.09	1.71%	19.93	1.17%	73.01	0.98%	6.13	5.60%	13.99	1.35%
PWR15	862	0.38%	5.36	1.51%	9.36	1.06%	33.51	0.69%	ND	NA	0.69	8.66%
PWR16	1038	0.33%	10.07	1.50%	18.21	0.95%	65.77	0.68%	3.47	7.23%	8.82	1.39%
PWR17	1086	0.15%	13.75	0.58%	23.92	0.40%	86.21	0.29%	12.14	1.26%	29.97	0.35%
PWR18	929	0.40%	8.46	1.54%	15.04	1.02%	54.03	0.99%	1.51	17.6%	4.27	2.51%
PWR19	672	0.34%	3.21	1.60%	5.73	1.13%	20.45	0.67%	ND	NA	0.25	16.7%
PWR20	714	0.29%	3.84	1.35%	6.73	0.96%	23.71	0.52%	ND	NA	0.38	10.2%
PWR21	700	0.47%	3.81	2.13%	6.87	1.41%	24.18	1.12%	ND	NA	0.36	16.6%
PWR22	646	0.43%	3.48	2.23%	6.20	1.51%	21.39	1.42%	ND	NA	0.40	14.4%
PWR23	728	0.37%	6.01	1.76%	10.92	1.12%	39.67	0.79%	2.55	8.49%	5.93	1.64%
PWR24	477	0.44%	4.06	1.43%	7.28	0.98%	26.39	0.67%	ND	NA	1.33	3.41%
BWR1	3628	0.20%	34.02	1.10%	60.81	0.73%	184.2	0.49%	290.3	0.41%	522.6	0.34%
BWR2	3333	0.27%	30.23	1.31%	51.74	0.90%	160.1	0.49%	175.2	0.64%	310.6	0.49%
BWR3	3205	0.32%	25.42	1.29%	44.67	0.87%	137.0	0.60%	82.4	1.06%	145.6	0.53%
BWR4	3008	0.30%	24.84	1.25%	43.82	0.84%	132.4	0.63%	70.4	1.16%	126.9	0.50%
BWR5	3299	0.27%	31.98	1.33%	56.92	0.87%	168.6	0.58%	265.2	0.47%	478.3	0.38%
BWR6	1665	0.31%	5.98	1.50%	10.58	0.99%	32.79	0.58%	ND	NA	0.56	13.0%
BWR7	3146	0.28%	27.89	1.25%	49.43	0.82%	150.1	0.51%	151.0	0.64%	272.4	0.43%
BWR8	3056	0.26%	32.71	1.12%	57.78	0.74%	178.0	0.47%	240.1	0.47%	439.5	0.36%
BWR9	3227	0.27%	32.22	1.39%	55.73	0.91%	171.0	0.59%	364.4	0.43%	655.8	0.41%
BWR10	3138	0.21%	34.59	1.10%	60.21	0.75%	181.4	0.46%	328.2	0.38%	591.3	0.33%
BWR11	1485	0.27%	7.20	1.16%	12.61	0.79%	39.15	0.48%	ND	NA	2.33	2.95%
BWR12	2564	0.29%	26.88	1.22%	47.01	0.82%	140.6	0.65%	157.2	0.58%	285.7	0.39%
BWR13	2778	0.26%	29.00	1.25%	50.95	0.87%	153.7	0.59%	183.9	0.58%	327.2	0.46%
BWR14	1310	0.29%	4.16	1.56%	7.40	1.03%	23.22	0.66%	ND	NA	0.27	20.0%
BWR15	1336	0.28%	5.09	1.27%	8.75	0.85%	27.03	0.54%	ND	NA	0.84	6.08%
BWR16	1225	0.29%	4.31	1.80%	7.67	1.21%	24.14	0.75%	ND	NA	0.44	14.1%
BWR17	1349	0.29%	5.09	1.65%	9.02	1.15%	28.66	0.68%	ND	NA	0.44	12.4%
BWR18	1011	0.27%	4.28	1.66%	7.85	1.07%	24.11	0.66%	ND	NA	1.41	4.12%
BWR19	1513	0.29%	6.43	1.21%	11.34	0.80%	34.64	0.52%	ND	NA	1.25	5.08%
BWR20	2090	0.28%	19.94	1.20%	34.43	0.82%	106.0	0.50%	129.3	0.57%	230.4	0.43%
BWR21	1110	0.29%	4.01	1.59%	7.01	1.09%	22.49	0.60%	ND	NA	0.41	10.3%
BWR22	1580	0.34%	11.19	1.97%	19.58	1.32%	59.01	0.88%	66.64	0.96%	120.2	0.64%
BWR23	1254	0.22%	6.46	1.78%	11.75	1.12%	37.76	0.51%	45.24	0.71%	78.08	0.67%
BWR24	619	0.42%	1.69	2.35%	2.96	1.61%	9.14	1.19%	ND	NA	0.23	14.1%
BWR25	404	0.36%	0.76	3.05%	1.35	1.95%	4.05	1.45%	ND	NA	0.14	13.9%
PWR25	395	0.39%	1.58	2.11%	2.87	1.40%	9.88	0.98%	ND	NA	0	NA

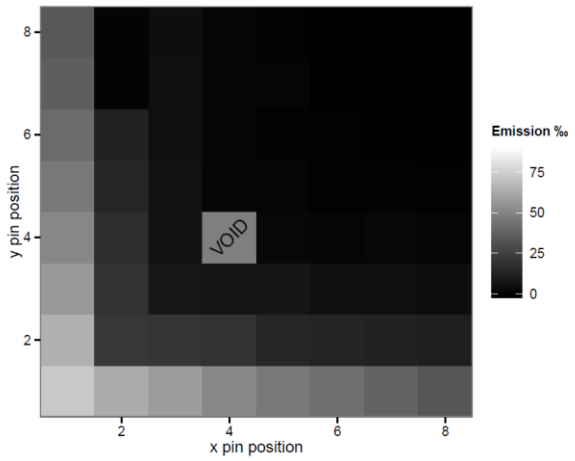

253 (662 keV)

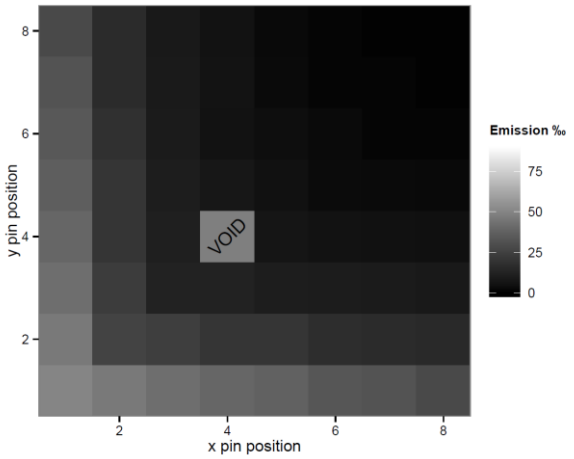

254 (1274 keV)

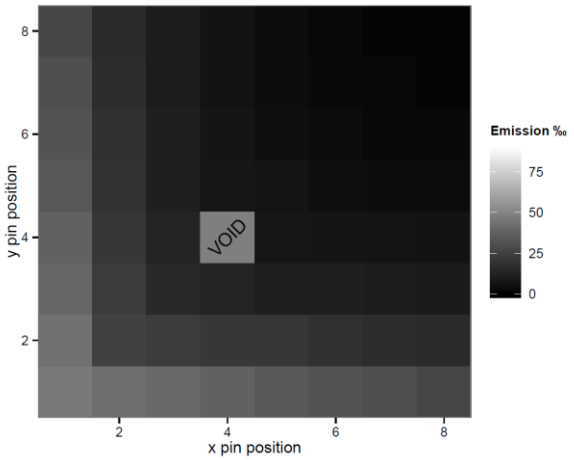

255 (1596 keV)

256 **Figure 4. Distribution of the contribution to the gamma-ray flux density of the full-energy peak, at the**
257 **detector position from an 8×8 assembly as calculated by Jansson [8]. The detector position corresponds to the**
258 **lower left corner. The contributions are shown as parts per thousand of the radiation emitted by the assembly**
259 **at that energy.**
260
261

3.3. Comparison of data from the two experimental setups deployed at Clab

As mentioned previously, four campaigns, two for PWR and two for BWR fuel assemblies, were carried out in 2013 and 2014 using two different detectors. During the first two campaigns, 25 PWRs and 17 BWRs were measured. A comparison of the areas for the ^{137}Cs 662-keV peak measured with the two different HPGe detectors is illustrated in Figures 5 and 6 for the PWR and BWR assemblies, respectively. Once the fuel is removed from the reactor, existing contributions from all other radioactive decay processes (mostly spontaneous and induced fission) can be considered as negligible for the spectral lines of interest, hence peak intensities were recalculated by simple half-life correction to the date of discharge from the reactor.

Although the measurements in both of these figures were taken for the same corner of the assembly, they were not taken for the same axial location. In the case of the PWR assemblies, the two locations were on opposite sides of the burnup plateau, separated by ~120 cm (see Figure 1). All measurements were made on the burnup plateau; an example of which is illustrated in Figure 8. For the latter two campaigns, from which the data was extracted for future analysis, the measurement position was 1.35 +/- 0.1 meters down from the top of the fuel. The small variability of the measurement location about the 1.35 m level was to avoid measuring on a spacer grid. The later two campaigns benefited from lessons-learned in the first two campaigns; the movement of the axial location measured to the 1.35 m location saved several minutes of fuel movement time per assembly. Moreover, different attenuator layers were used (see Table 3).

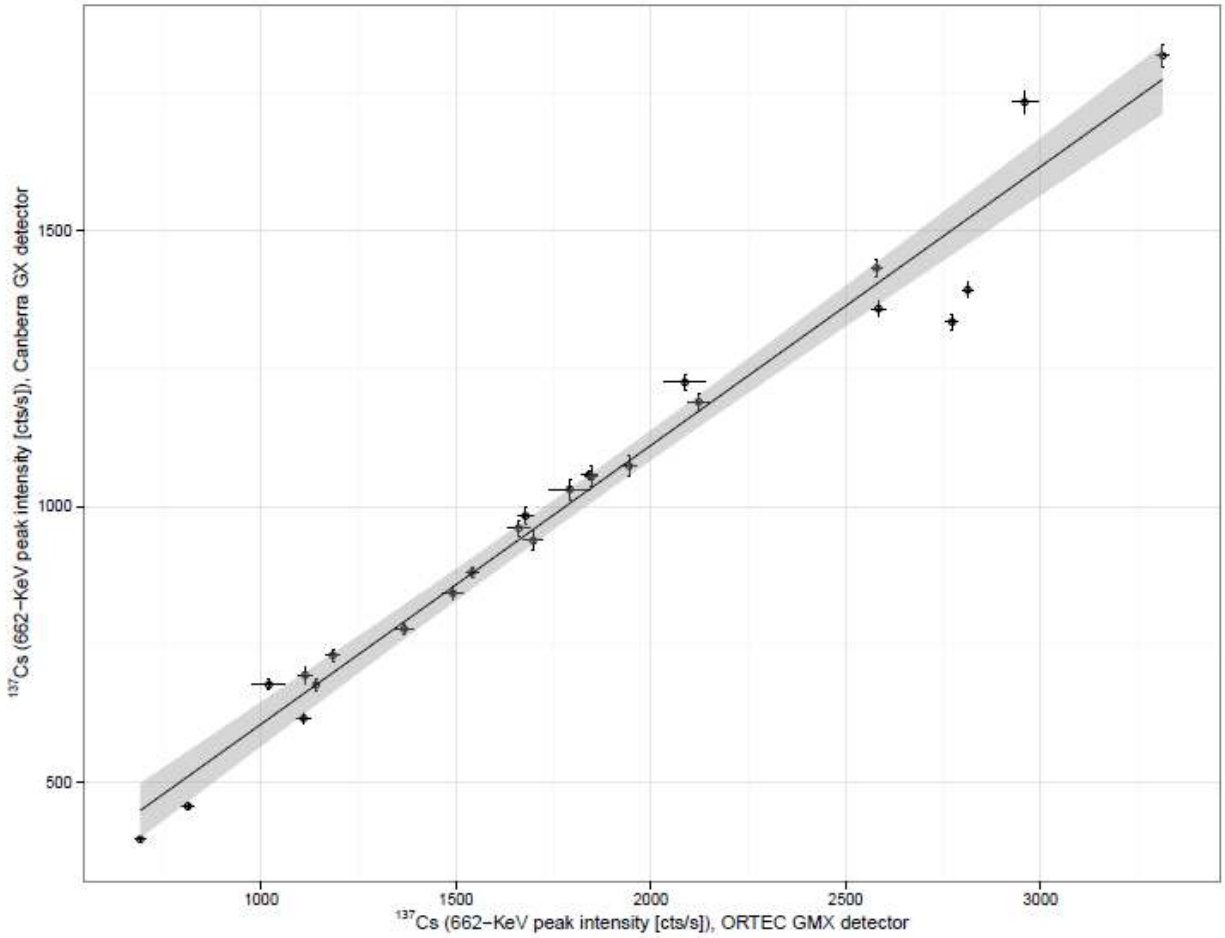

Figure 5. The 662-keV net peak area from ^{137}Cs, which was measured with the ORTEC GMX detector and Canberra Lynx MCA, from the 45-degree corner at an axial location of ~260 cm down from the top of the PWR fuel is presented. This area is compared with the measurement of the same peak, which was taken with the Canberra GX detector and GBS Elektroniks' MCA-527, for the same corner but at a difference axial location, ~140 cm down from the top of the fuel (when not visible, the uncertainty bars are smaller than the data points).

The shaded region around the curve fit of the data points depicted in Figures 5 and 6 represents the uncertainty of the linear model, assessed as the variability (standard error) in the estimate for the model coefficients [19][20]. Each point's measurement uncertainty is purely estimated from counting statistics and for most data points is too small to be visible on the scale of the plots. The same approach to uncertainty depiction is used in all the graphs in this publication where trend lines are calculated.

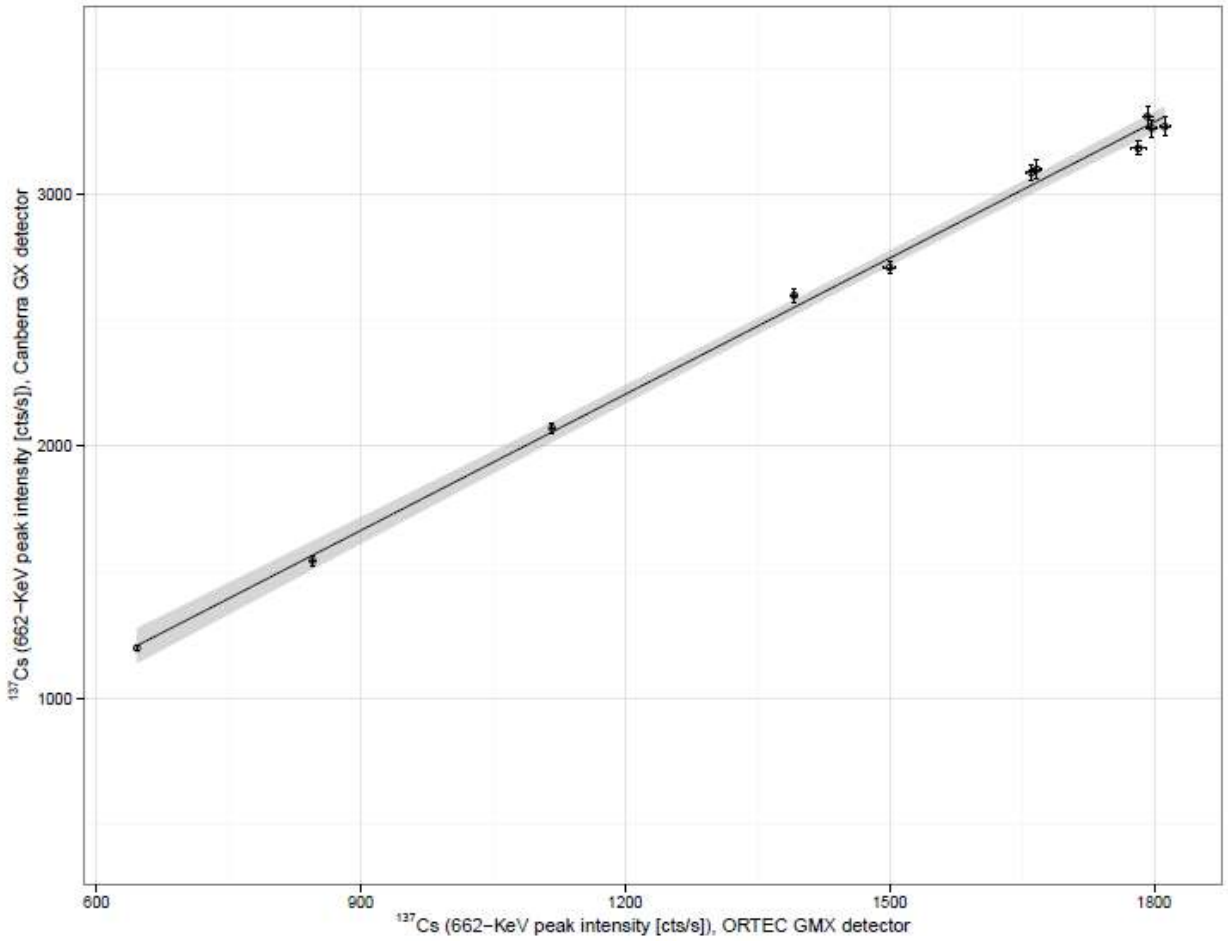

Figure 6. The 662-keV net peak area of 137Cs, which was measured with the ORTEC GMX detector and Canberra Lynx MCA, from the 45-degree corner at an axial location of ~153 cm down from the top of the BWR fuel, is shown. This area is compared with the measurement of the same peak, which was measured with the Canberra GX detector and GBS Elektroniks' MCA-527, for the same corner but at a difference axial location, which was ~138 cm down from the top of the fuel (when not visible, the error bars are smaller than the data points).

From Figures 5 and 6, the following observations can be made: (1) both passive gamma systems appear to be working as expected relative to each other given the linear relationship in the net peak area measured from the same assemblies. (2) The noted variation from the linear fit is significantly greater among the PWR assemblies as compared with the BWR assemblies. It is expected that this variation occurs primarily because the measurement locations for the PWR assemblies were on opposite sides of the burnup plateau, ~120 cm apart, whereas the BWR measurement locations were separated by an axial distance of only ~15 cm. This variation is in accordance with what is presented in [9].

3.4. Characteristic change in isotope abundance with burnup

The relation between the spectral peak areas and reactor operation for all 50 assemblies is central to this study. In particular, the relation among the most intense gamma peaks (137Cs, 154Eu, and 134Cs) as a function of the average assembly burnup is illustrated in Figure 7. To illustrate the burnup dependency, the net peak areas were recalculated to the time of discharge from the reactor, taking into account only the exponential decay of these isotopes with cooling time.

As a starting point for explaining the observed net peak areas, the buildup of ^{134}Cs, ^{137}Cs, and ^{154}Eu upon discharge from the reactor is shown in Figure 7. The buildup of the ^{134}Cs, ^{137}Cs, and ^{154}Eu activity as a function of fuel burnup for a representative BWR was calculated by ORIGEN-ARP [21], assuming the reactor's specific power as constant throughout the irradiation. The calculation used the declared burnup and initial enrichment for BWR10, as well as typical reactor operating scenarios; detailed reactor operating data for this specific assembly was not used. In fact, a more detailed simulation of the specific assembly requires a more complex code than ORIGEN-ARP and is outside the scope of the current paper. The assembly represented in Figure 7 is a 10×10 assembly, with an initial enrichment of 3.144% and a burnup of 39.5 GWd/MTU; it was irradiated for five consecutive cycles (e.g., without intermediate cooling beyond the duration of a typical intercycle shutdown).

The increase in the ^{134}Cs, ^{137}Cs, and ^{154}Eu activity as a function of fuel burnup, as illustrated in Figure 7, reflects the typical trends for these isotopes observed in the power reactor context [6], [22],[23]. The production of ^{137}Cs is known to be nearly linear with burnup in the considered range because ^{137}Cs is primarily a direct fission product, and the production yields of ^{137}Cs from the fission of ^{235}U, ^{239}Pu, and ^{241}Pu are similar. The more complex variation in ^{134}Cs and ^{154}Eu is also illustrated. The data depicted in Figure 7 are based on the results of a simplified simulation, (e.g. for one particular assembly irradiated in one particular reactor operating scenario); a different initial enrichment or a variation in reactor operation may cause a different pattern in the isotopic evolution. However, Figure 7 is a useful starting point for interpreting the experimental data in the next section.

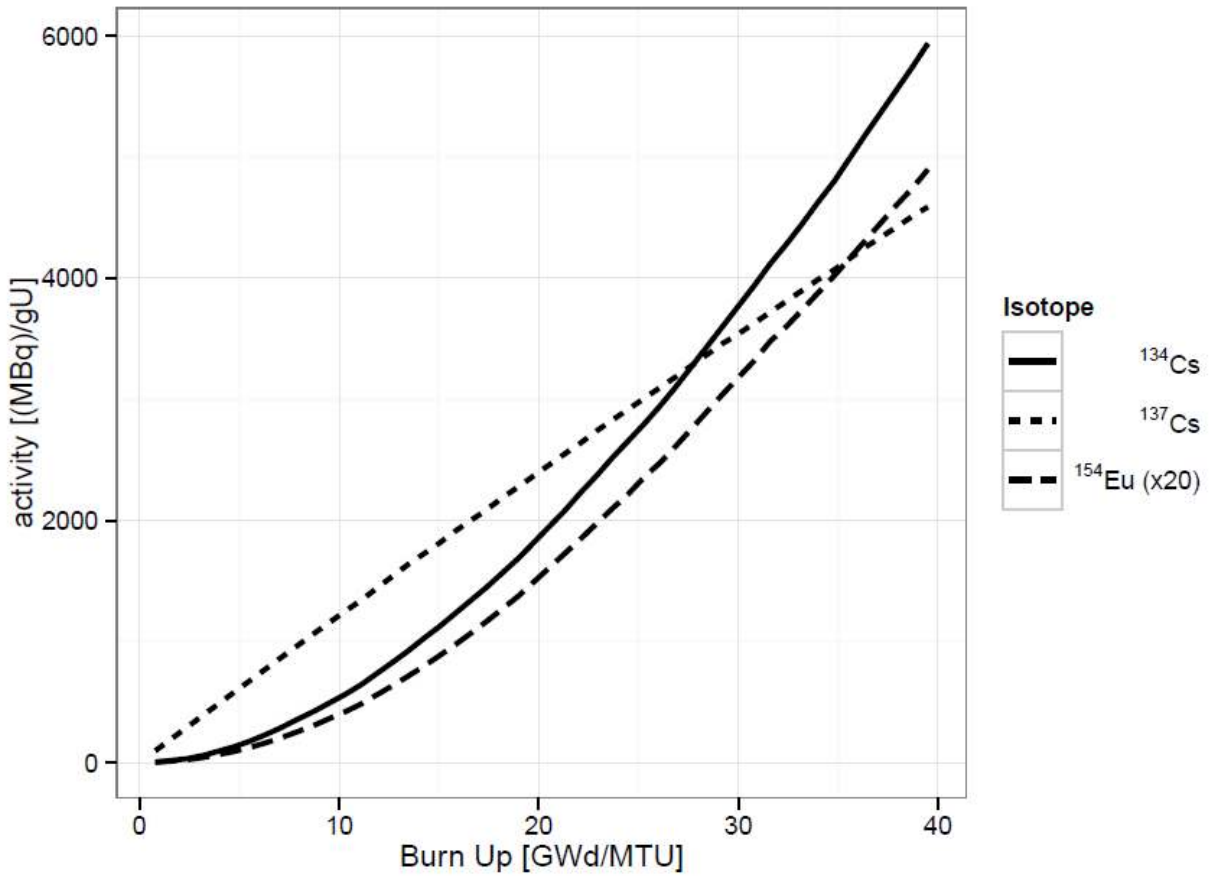

Figure 7. The buildup of the 134Cs, 137Cs, and 154Eu activity as a function of fuel burnup for BWR10 (assuming the reactor's specific power as constant throughout the irradiation), as calculated by ORIGEN-ARP.

3.5. Axial variation

Although the primary focus of this paper involves illustrating the variation in the dominant peaks from ^{134}Cs, ^{137}Cs, and ^{154}Eu as a function of the 50 assemblies measured, it is important to emphasize that the data presented in Figure 9 to 16 are given from a fixed axial location on the fuel that extends only 1.5 cm in the vertical direction. Furthermore, in Figures 7 to 14 we are comparing this localized measurement with the burnup of the fuel, which is a quantity that was determined for the full ~3.7-m length of the assembly. In Figures 4 and 5, when the two measurement systems were compared, we noted that measurements made 15 cm apart had better agreement than those made 120 cm apart. This fact motivated a graph to illustrate the burnup variation, as represented by the ^{137}Cs peak intensity, along the assembly.

In Figure 8, the ^{137}Cs intensity measured from 34 separate static measurements along the 45-degree corner of BWR9 is illustrated. At the ends of the assembly, the fuel was moved in intervals of ~8 cm between measurements, whereas on the plateau it was moved in intervals of ~16 cm. The ORTEC GMX detector and Canberra Lynx MCA were used.

In Figure 8, the amount to which the ^{137}Cs intensity can vary over distances of 15 and 120 cm along the plateau is clear. More importantly, the increased variation evident in Figure 5 as compared with Figure 6 can be understood by observing the variation of the shape of the plateau region among assemblies.

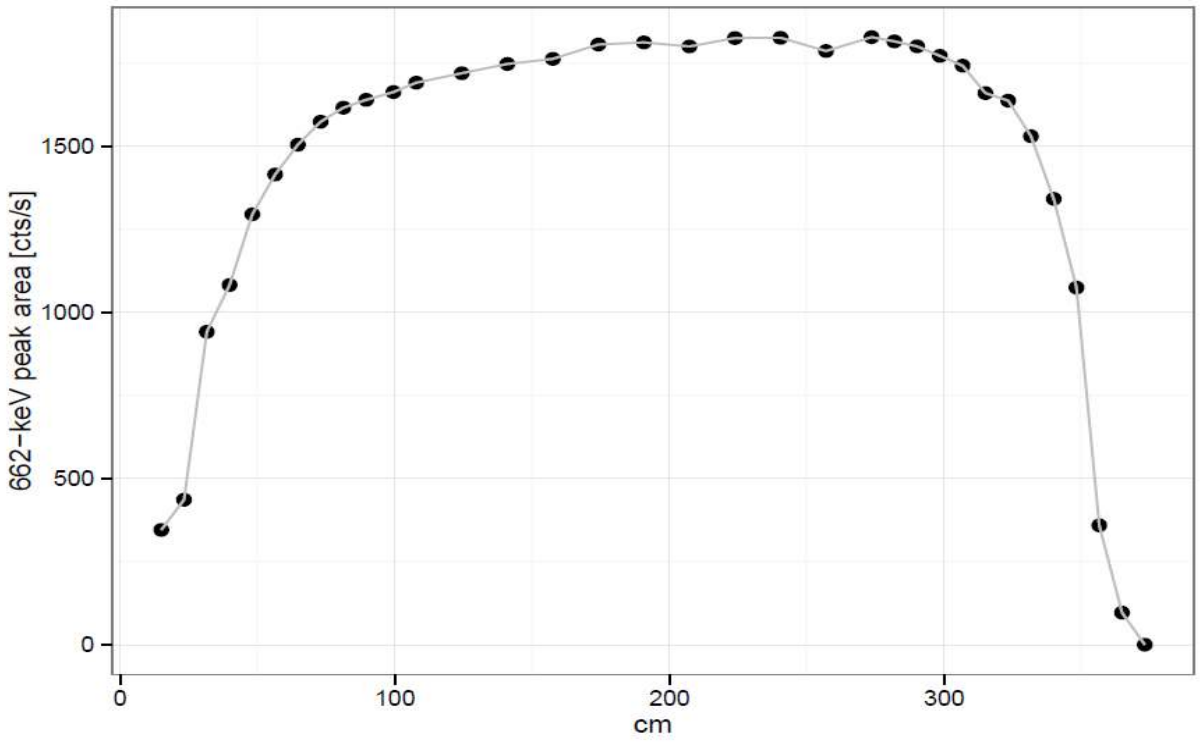

Figure 8. Count rate for the 662-keV 137Cs net peak area as a function of axial location along BWR9. These data were measured with the ORTEC GMX detector and Canberra Lynx MCA from the 45-degree corner. The axial location is specified as downward along the uranium containing portion of the fuel (The indicated absolute positions are accurate to ±10 cm, the error bars are much smaller than the data points).

3.6. Variation in measured peak intensity of ^{137}Cs, ^{154}Eu, and ^{134}Cs with burnup

One of the goals of our collaborative research effort is to quantify the relative usefulness among a range of passive gamma-ray measurement options, following the experimental plan described in paragraph 2.2.

In particular, we want to quantify the benefit of measuring the gamma intensity from a single corner, as compared with a combined measurement on opposite corners (i.e. performing a 180° rotation of the fuel after having measured one corner), as compared with a combined measurement of all assembiely's four corners. Additionally, these three options will be tested for both static measurements (i.e. at a fixed level) and measurements that scan the entire length of the assembly. The current publication is a starting point along the research path to answer these questions. We plan to use various combinations of the passive gamma data, combined with signals from other NDA instruments, to find optimal solutions for the five technical goals outlined in the introduction.

Except where indicated otherwise, the data presented in this paper are the net peak area count rates averaged for the four corners measured with the Canberra GX detector and GBS Elektroniks' MCA-527. Also, unless noted otherwise, the axial locations measured were ~140 cm and ~138 cm down from the point from which radiation from ^{137}Cs was first detected from the fuel, respectively, for PWRs and BWRs. It is anticipated that averaging among the corners will be beneficial in achieving our technical goals because all of these goals involve properties of the entire assembly. For example, the declared burnup value compared with in this section is the average burnup of the entire assembly.

In Figure 9, the cooling-time-corrected count rates for the 662-keV peak of ^{137}Cs for the 25 PWR assemblies are illustrated. The data points are grouped according to their fuel type, as well as to the presence or absence of gadolinium-loaded rods. Even though the pin size and number of pins are different between the 15×15 and 17×17 assemblies, the two subgroups exhibit the same correlation between the ^{137}Cs peak area and burnup; all 15×15 assemblies are within two sigma of the best fit, with three assemblies falling above the regression line and two below the line. Also, the presence of some gadolinium rods in an assembly does not appear to bias the assembly; three assemblies with gadolinium rods fell above the best-fit line, and four assemblies fell below the line. For the PWR24 assembly, the ^{137}Cs intensity is estimated by the best-fit curve further from the measured data point; a count rate of ~500 counts per second (cps) was measured, whereas ~730 cps is predicted by the best fit. This variation is not

surprising given that this assembly was in the core for two cycles, then removed for 10 years before being returned to the reactor for two cycles. Because the cooling-time correction is based on the date of discharge, the ^{137}Cs produced during the first two cycles decayed significantly more than was accounted for by this correction, even considering the 30-year half-life of ^{137}Cs; thus, it is not surprising that the measured value for PWR24 deviated from the regression line when compared with the other assemblies that all had more typical reactor histories. In Figure 9 and in some of the subsequent graphs (Figure 10 and Figures 17 to 19) the intercept was forced to 0. This choice is consistent with the fact that, in an environment with a negligible background at those specific energies, a fresh fuel assembly with a burnup of zero does not contain any fission products, nor does it emit spent fuel characteristic gamma-ray lines. From the data observed, this assumption can be considered as legitimate because, when excluding the zero intercept constraint, the standard error on the intercept was smaller than its value (Student's t-test <1).

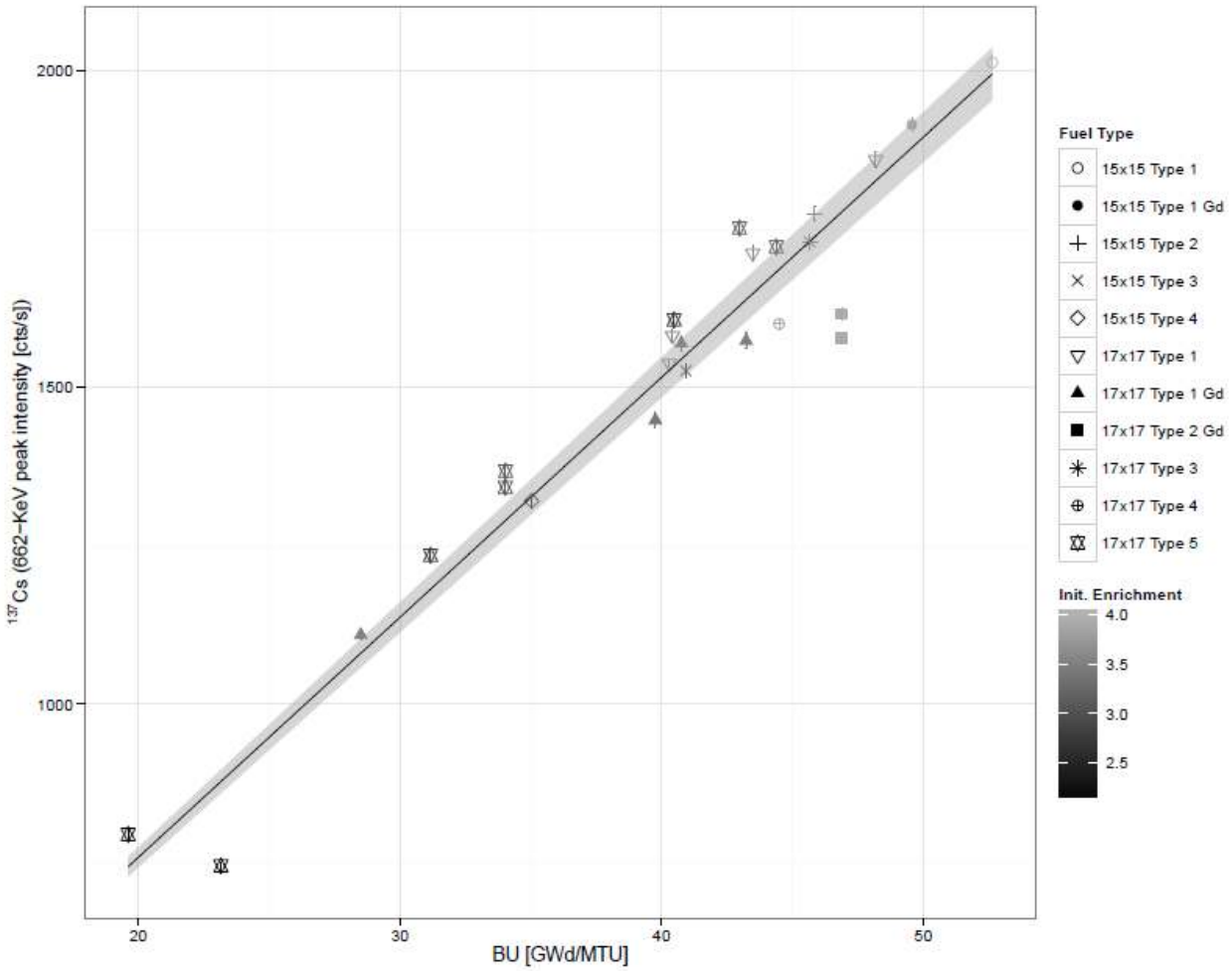

Figure 9. The peak area of 662 keV from ^{137}Cs is depicted as a function of burnup for the measured PWR assemblies. The error bars and the shading around the regression lines correspond to the standard error on the linear fit's coefficients at the 95% confidence level (when not visible, the error bars are smaller than the data points).

In Figure 9, the BWR data for ^{137}Cs as a function of burnup is illustrated. For these assemblies, the division is clear among assembly types. The 8×8 assemblies clearly have a different regression line compared with the 10×10 assemblies. This difference is not surprising given that the two groups of assemblies are different in their uranium pellet diameters. The 8×8 assemblies have fuel rods with 10.44-mm diameters, whereas the 10×10 assembly rods have 8.19-mm diameters [24]; however, the exterior size of the assemblies is nearly the same. The 15×15 and 17×17 PWR assemblies have a smaller pellet diameter difference of 9.3 mm and 8.17 mm, respectively. It appears from the measured data that this smaller-diameter difference, combined with other features specific to the PWR fuel (e.g., the more

densely packed assembly structure), make all the PWR assemblies trend similarly with respect to the ^{137}Cs count rate vs. burnup data. The difference in the pellet diameter impacts many factors: (1) the actual irradiation in the reactor is altered because the assemblies with smaller-diameter pellets also have more water around each pin relative to the larger pellets; thus, a lower-energy neutron spectrum exists in the 8×8 assemblies; (2) since the dominant contribution to the detected gamma rays is from the outermost pins (see figure 2), in-pin self-attenuation, more relevant on thicker pellets, can affect lower energy peaks' intensity; and (3) the different assemblies do not have the same mass per unit vertical length, nor does a unit mass experience the same irradiation as a function of distance inside a pellet; thus, the production of ^{137}Cs between the two cases is not easy to discern. The measured spectra are impacted by the combined influence of all these factors and possibly others that are less evident.

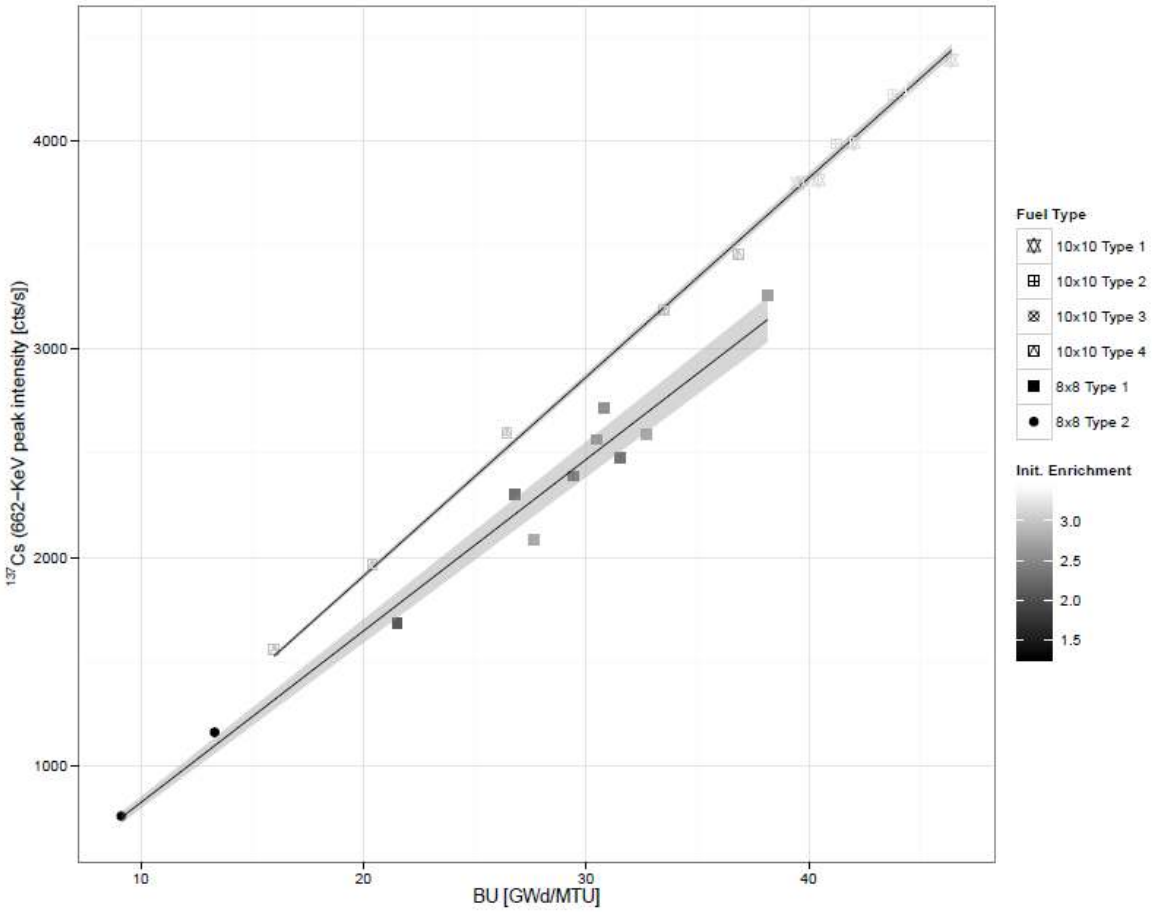

Figure 10. The peak area of the 662 keV from ^{137}Cs is depicted as a function of burnup for BWR assemblies. Two separate regression lines are used: one for the 10×10 assemblies and one for the 8×8 assemblies (when not visible, the error bars are smaller than the data points).

Despite the fact that the irradiation of BWR assemblies is inherently more complex than PWRs and that more of the BWR assemblies experience at least one cycle out of the reactor between the first and last cycles in the reactor, scatter in general is less about the respective regression line for BWRs as compared with the PWRs. In Table 2, four of the BWR assemblies are indicated as experiencing abnormally longer irradiation histories: more than 11 years passed between the assembly first entering the reactor and finally being discharged. All four of these assemblies were 8×8s and are the four data points that have measured count rates just below the 2 sigma uncertainty band in Figure 10. As was noted for the single PWR assembly with a similarly long irradiation history, the oversimplification of the cooling-time correction, using the discharge date rather than the date a certain isotope was created, is expected as the primary reason for this result.

As mentioned earlier, the detection of gamma rays from ^{154}Eu, given its relatively long half-life of 8.6 years, may be the primary design criterion for the passive gamma system at the Clink facility. For the measurement system used in the current research (2.5-m fuel-to-detector separation and HPGe detector) the uncertainty of the 1274-keV line of ^{154}Eu for a ~27-year-cooled, ~30-GWd/tU-burned BWR assembly was 1.5% for an ~8-minute live time with a single crystal. In designing a passive gamma system for Clink, the designer can use attenuation, collimation and distance to keep the count rate within the operating regime of a given detector. In the case of Clink, with fuel cooled for 10 years or more, there is some flexibility in the selection of the detection material. A crystal such as LaBr3 has sufficient resolution for the peaks of interest; this is an important point given that LaBr3 can tolerate much higher count rates relative to HPGe. As a result, the detector can be positioned closer to the fuel. Furthermore, attenuation rather than collimation and distance can be used to manage the count rate of the detector. This is desirable in the context of measuring the 1274-keV line because the mass attenuation coefficient of most gamma attenuating materials are much higher below ~1 MeV. Hence, attenuation as a means of count rate management will the percentage of 1274-keV photons reaching the fuel relative to 662 keV

463 photons of Compton scattered photons. As a result it is anticipated that the 1274-keV keV line can be
464 detected from fuel with cooling time of ~60 years.
465 Unlike ^{137}Cs, ^{154}Eu production is complex and is not directly produced in significant quantities from
466 fission. In fact, for uranium, more than 20 reaction chains lead to ^{154}Eu production [22],[23]. In Figure 11
467 11, the intensity of the 1274-keV line of ^{154}Eu is illustrated as a function of burnup for the 25 PWR
468 assemblies, whereas in Figure 12, the same graphs for the 25 BWR assemblies are illustrated. The trend is
469 consistent with the variation illustrated in Figure 4. A slight quadratic trend is evident >20 GWd/tU for
470 the PWR assemblies, whereas for BWR assemblies, the trend appears to be closer to linear.
471
472 The interpretation of the 154Eu net peak area, relative to the ^{137}Cs peak area, is complicated by not only
473 the large range of production mechanisms, which render it more sensitive to reactor operation, but also by
474 the relatively shorter half-life, which makes 154Eu more sensitive than ^{137}Cs to inaccuracies in the
475 cooling-time correction. An additional difference is that the 1274-keV line of 154Eu is significantly more
476 penetrating than the 662-keV line of ^{137}Cs; thus, the detected 1274-keV photons from 154Eu come from
477 interior pins more than the 662-keV photons from ^{137}Cs, as illustrated in Figure 4. The following changes
478 were noted among the assemblies as the analysis moved from the 662 keV line to the 1274 keV line: (1)
479 PWR24, the assembly with a 14-year difference between first entering a reactor and final discharge, is
480 now within the 95% confidence interval, while for the 662 KeV line of 137Cs PWR24 was > 5 sigma
481 from the regression line; Also, (2) BWR11, BWR17, BWR18, and BWR21 are not consistently low
482 relative to the trend line, as was the case with 137Cs. Because these assemblies do not vary in a manner
483 consistent with a cooling-time variation, it is suggested that factors other than cooling time are more
484 significant in these cases.

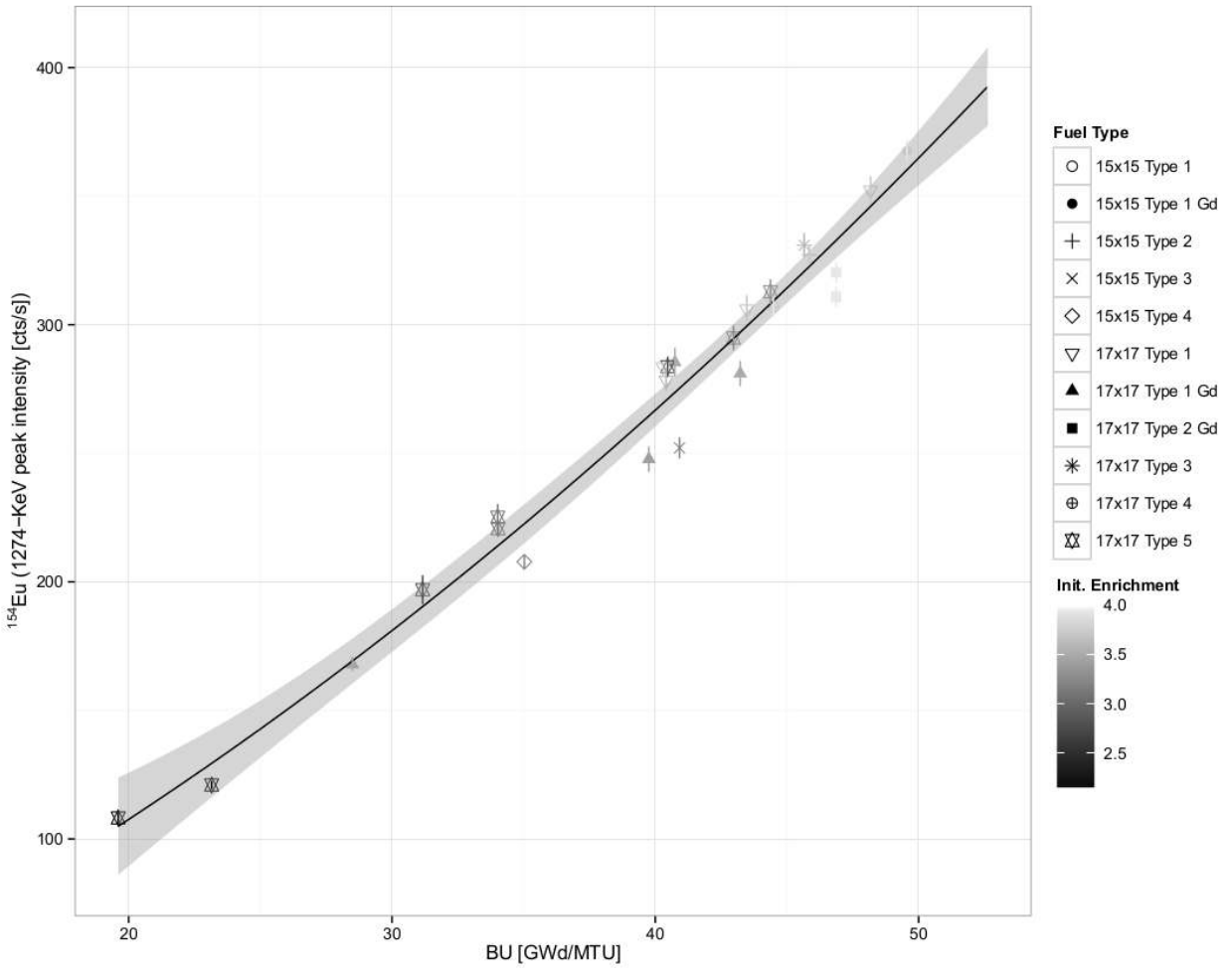

Figure 11. Variation in the 1274-keV peak intensity of ^{154}Eu as a function of burnup for PWR assemblies. The trend line represents a quadratic fit (when not visible, the error bars are smaller than the data points).

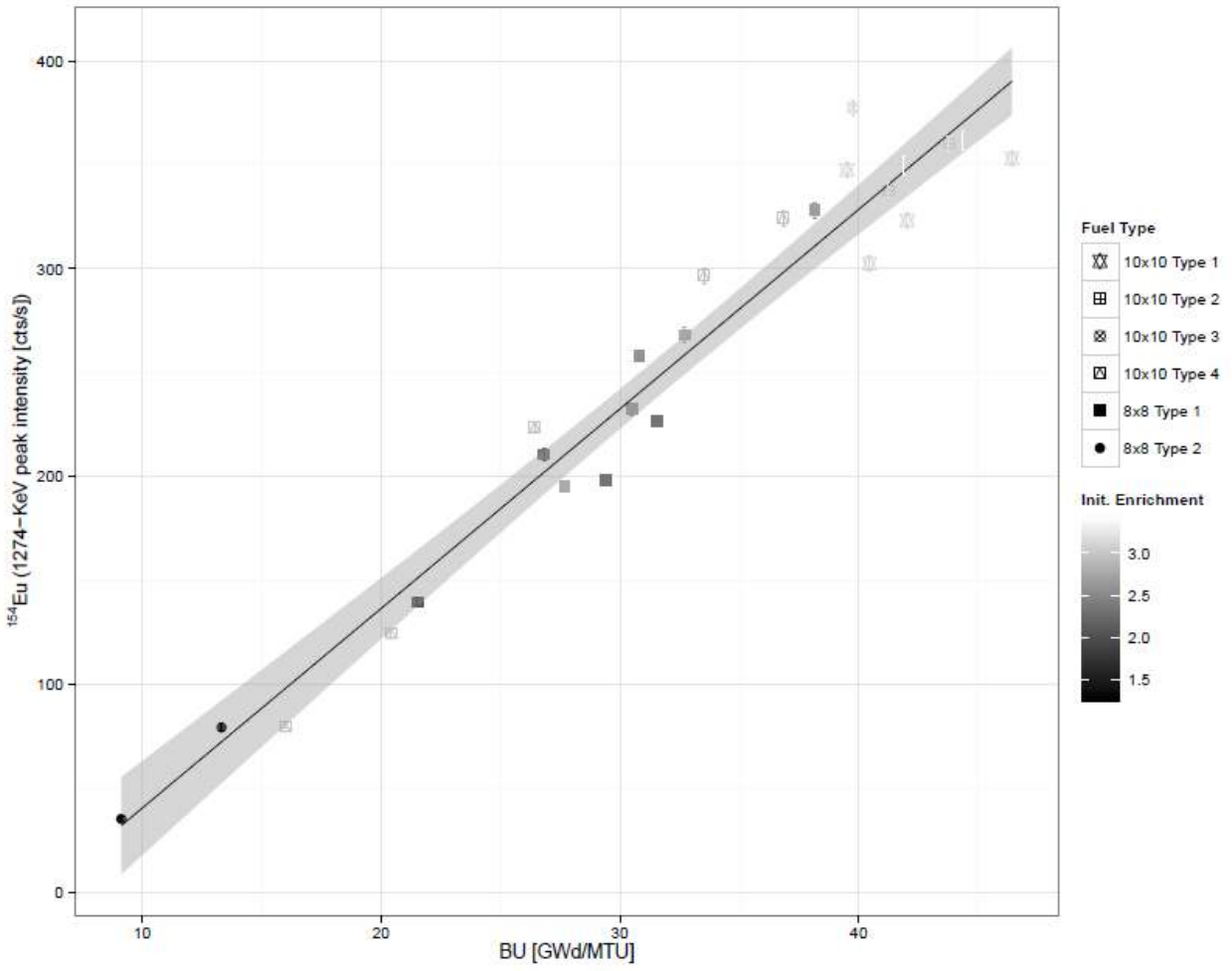

Figure 12. Variation in the 1274-keV peak intensity of ^{154}Eu as a function of burnup for BWR assemblies. The trend line represents a linear fit (when not visible, the error bars are smaller than the data points).

The 2.1-year half-life of ^{134}Cs is expected to limit the usefulness of this isotope for encapsulation facilities, even though it is a prominent peak in many spectra at relatively short cooling times. The production of ^{134}Cs is mainly due to neutron capture in ^{133}Cs, an isotope which is primarily produced from ^{133}I via ^{133}Xe. Almost independent of the fission source, ^{134}Cs is expected to depend roughly quadratic with the burnup [6], [23]. However, because of its short half-life, ^{134}Cs decays significantly both inside and outside the core; as a result, its isotopic content at a given moment in time is sensitive to reactor operation and time; in addition, the abundance of ^{134}Cs is sensitive to the energy spectra of the neutrons existing in the core.

The peak count rate for the strongest detected line from ^{134}Cs, the 796-keV line, is illustrated in Figures 13 and 14 for PWRs and BWRs, respectively. Given the large uncertainty due to counting statistics in several points, a geometric trend line would have considerable scatter. The BWRs exhibit a shape consistent with a quadratic increase with burnup, whereas for the PWR assemblies, such a trend is not evident. The points with the biggest uncertainties are those with a longer cooling time and consequent small peak-to-background ratio.

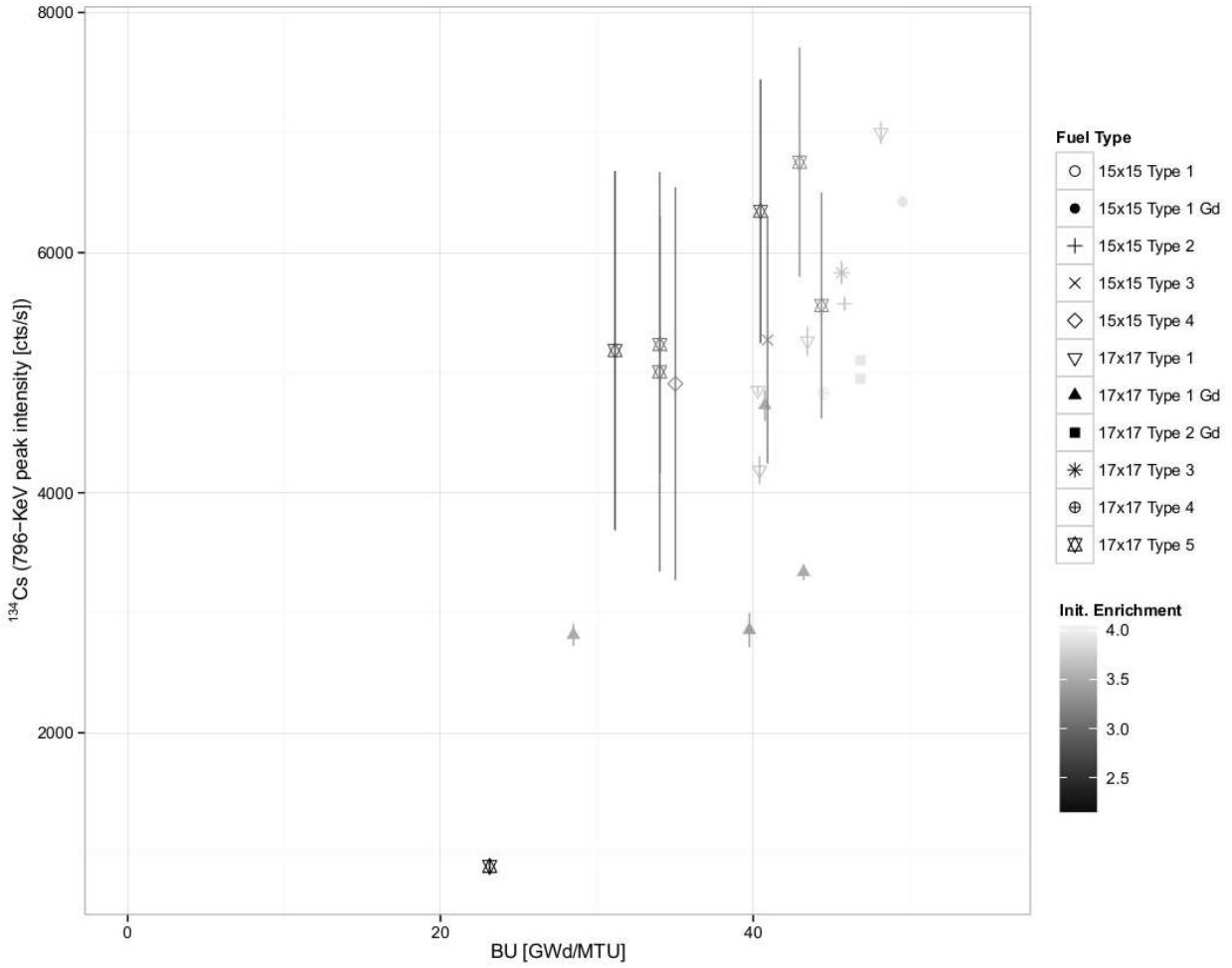

Figure 13. Variation in the 796-keV peak intensity of ^{134}Cs as a function of burnup for PWR assemblies (when not visible, the error bars are smaller than the data points).

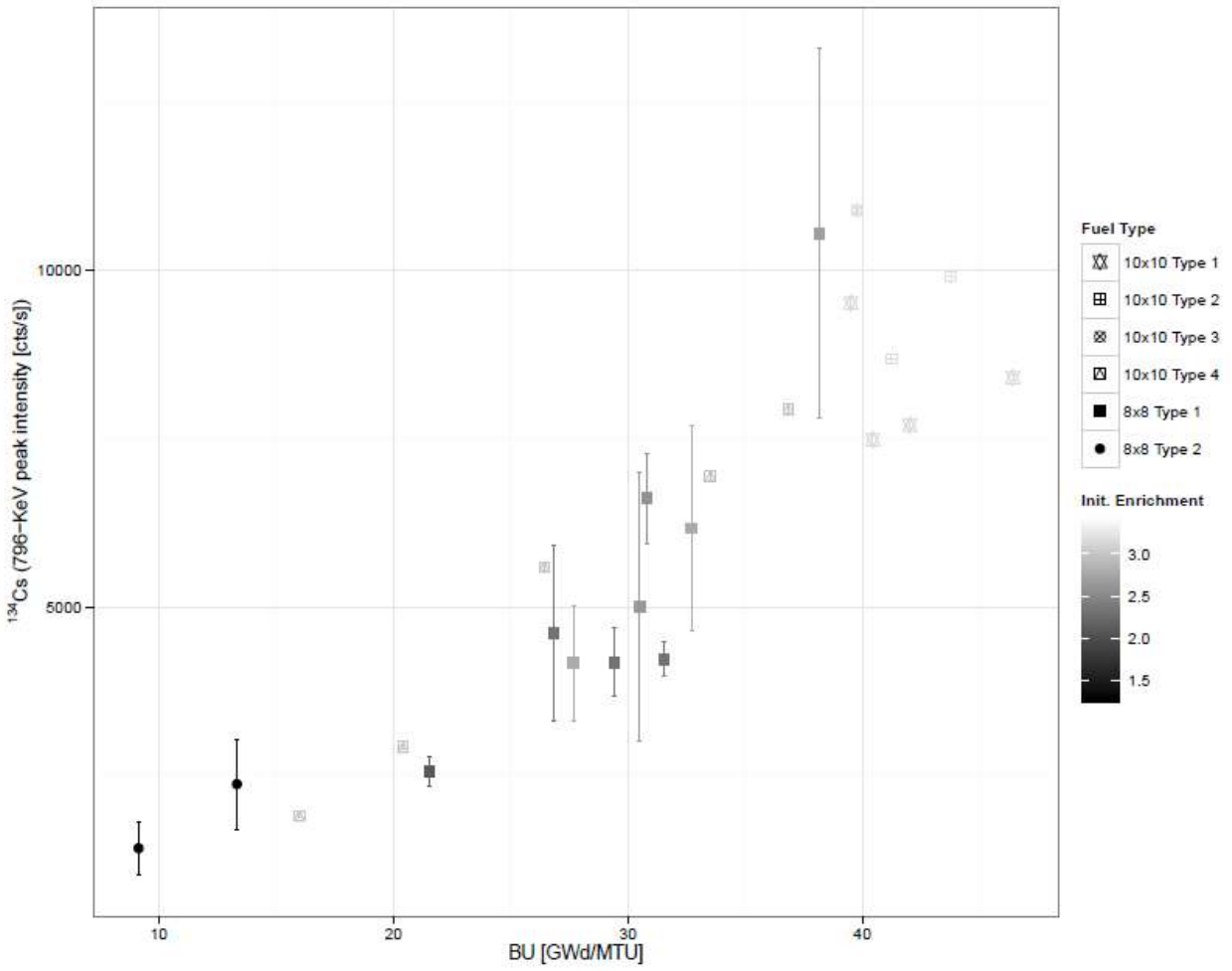

Figure 14. Variation in the 796-keV peak intensity of ^{134}Cs as a function of burnup for BWR assemblies (when not visible, the error bars are smaller than the data points).

3.7. ^{154}Eu/^{137}Cs characteristic peak variation burnup

The peak intensity ratios for ^{154}Eu/^{137}Cs and ^{134}Cs/^{137}Cs are frequently used when analyzing spent fuel spectra to characterize assemblies. In this section we present data for the ^{154}Eu/^{137}Cs given the significance of these two isotopes to our research plans.

The ratios of spectral lines are used in addition to the individual lines for several reasons. One reason is the relative insensitivity of ratios to variation in the detection efficiency due to the positioning of each fuel assembly relative to the detector because both the numerator and the denominator in the ratio vary

similarly. In the case of the Clink facility, uncertainty due to positioning is not expected to be significant because the fuel is expected to go through an opening that will allow for relatively tight position control. The $^{154}Eu/^{137}Cs$ ratio is nearly linear with burnup for fuel, with burnups under ~35 GWd/tU, as shown in both figures; therefore, the measured $^{154}Eu/^{137}Cs$ gamma ratio can be used to infer the fuel burnup, as long as the fuel is in the appropriate burnup range. Another feature of this ratio is that it transitions from linearly increasing to saturating/decreasing at burnups >~35 GWd/tU due to the combined effects of ^{239}Pu saturation and ^{154}Eu burnout at higher burnups [25]. Such saturation/decrease >35 GWd/tU is observed in the BWR data but not in the PWR data, which warrants further investigation.

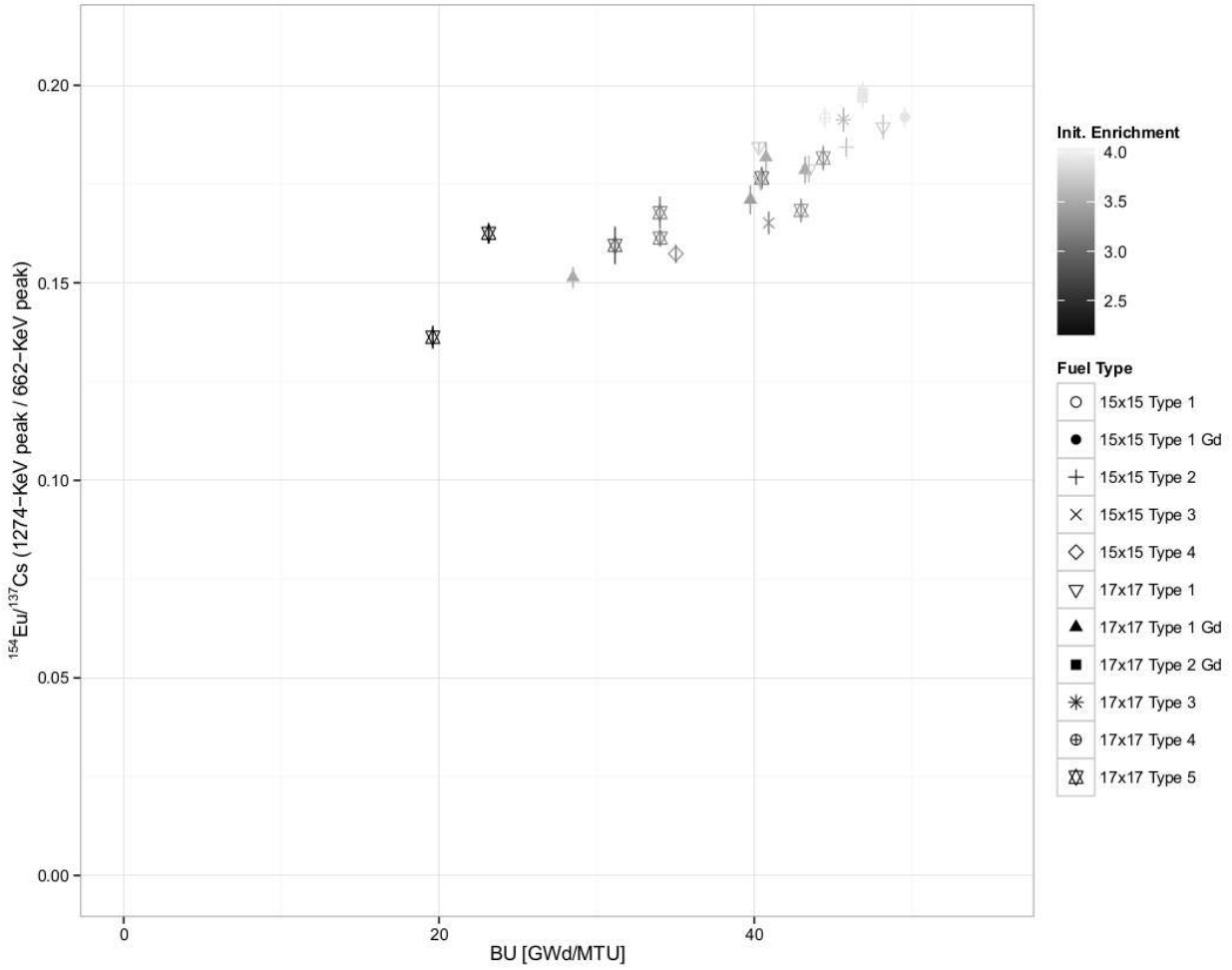

Figure 15. Variation in the ratio of $^{154}Eu(1274)/^{137}Cs(662)$ as a function of burnup for PWR assemblies (when not visible, the error bars are smaller than the data points).

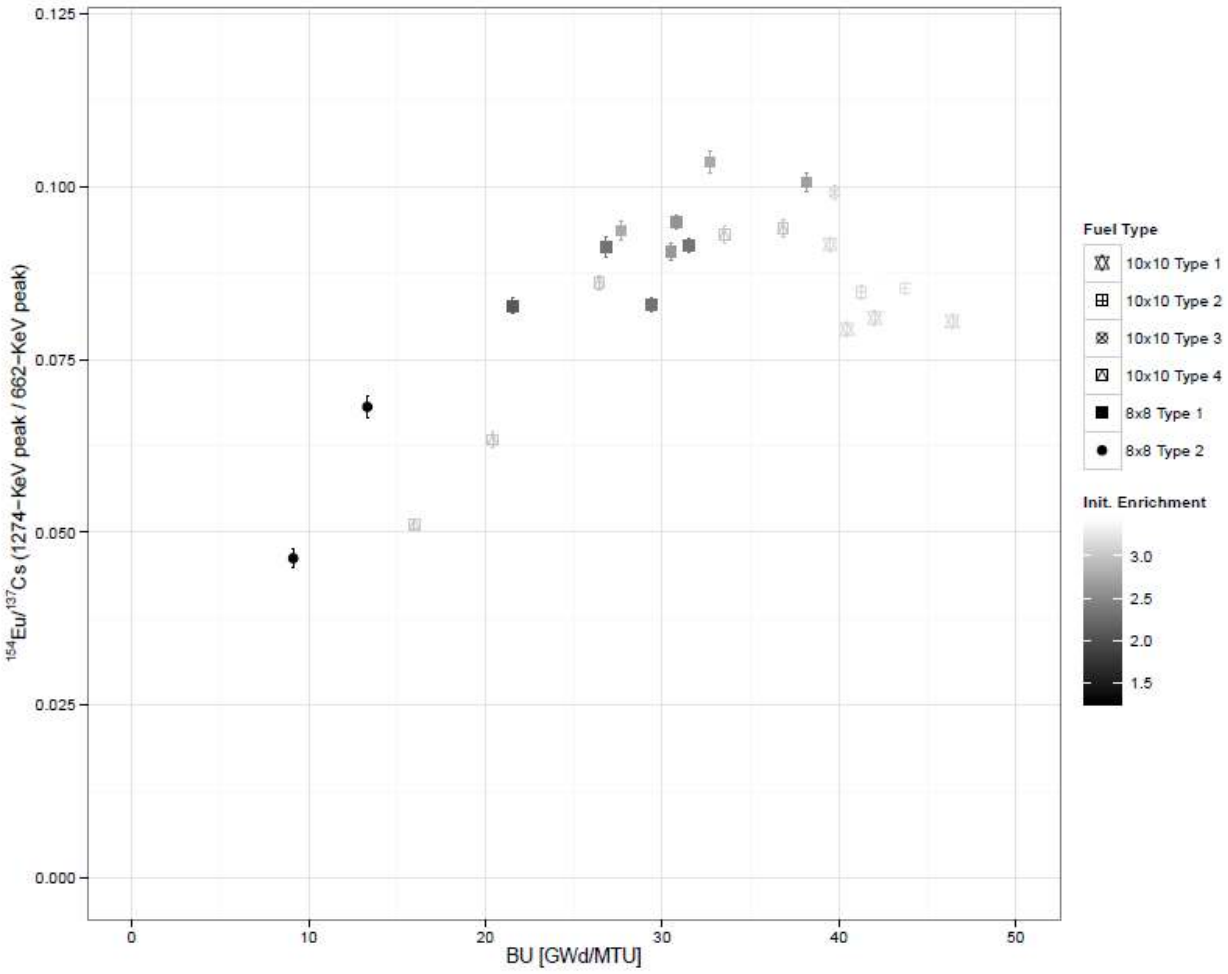

Figure 16. Variation in the ratio of 154Eu(1274)/137Cs(662) as a function of burnup for BWR assemblies (when not visible, the error bars are smaller than the data points).

3.8. Comparisons between measured peak intensities and calculated activities for the BWR dataset

A fundamental challenge in interpreting NDA signals from spent fuel is the shear complexity of reactor operation. Many factors (water temperature, fuel geometry, void formation, time in the reactor, power level of the reactor, control blade deployment, duration of inter-cycle shutdown, initial enrichment, use of burnable poisons, shuffling scenario, etc.) combine to determine the isotopic mixture in the assembly at discharge. This complexity impacts the production and destruction of different isotopes in different ways; this fact motivates the pattern recognition signal integration approach to be used. This complexity

552 highlights the uniqueness of the spectrally resolved passive gamma signal because the spectral lines of
553 specific isotopes can be separated from one another.
554
555 To compare the measured passive gamma results with theory, it is necessary to use tools made to quantify
556 the impact of all the various important factors. This comparison to theory will be accomplished by several
557 different publications. A more accurate calculation, using detailed information from the reactor operator,
558 is in preparation [23]; in the current publication, we did simple calculations based on total burn-up and
559 cooling time: these are the minimum data made available by the nuclear operator, on a mandatory base, in
560 his declaration to the safeguards inspectors. For the BWR dataset, ORIGEN-ARP [21] that contains fuel
561 libraries for specific fuel types was used for the irradiation and depletion calculation. In particular, we
562 operated ORIGEN-ARP in "Express" mode: this specific feature of the program allows quick irradiation
563 and depletion calculations with a limited amount of initial input information; therefore, it was suited to
564 calculate .the activities of ^{137}Cs, ^{134}Cs, and ^{154}Eu, with the information available were calculated. In
565 Figures 17, 18, and 19, the measured count rates from the most prominent line of each isotope are
566 graphed as a function of the activity of each isotopes calculated with ORIGEN-ARP. The assemblies
567 BWR19, BWR24, and BWR25 (all "first-cycle fuel") are excluded from this analysis because their initial
568 enrichment was outside the applicable range of the spent fuel libraries available. Because ORIGEN-ARP
569 can simulate both the irradiation and decay phases of the fuel evolution, the comparison includes the final
570 cooling in the simulation. The cluster of points around zero for ^{134}Cs and ^{154}Eu, corresponds to the oldest
571 assemblies for which those isotopes are almost completely decayed in Figures 17 and 18.
572

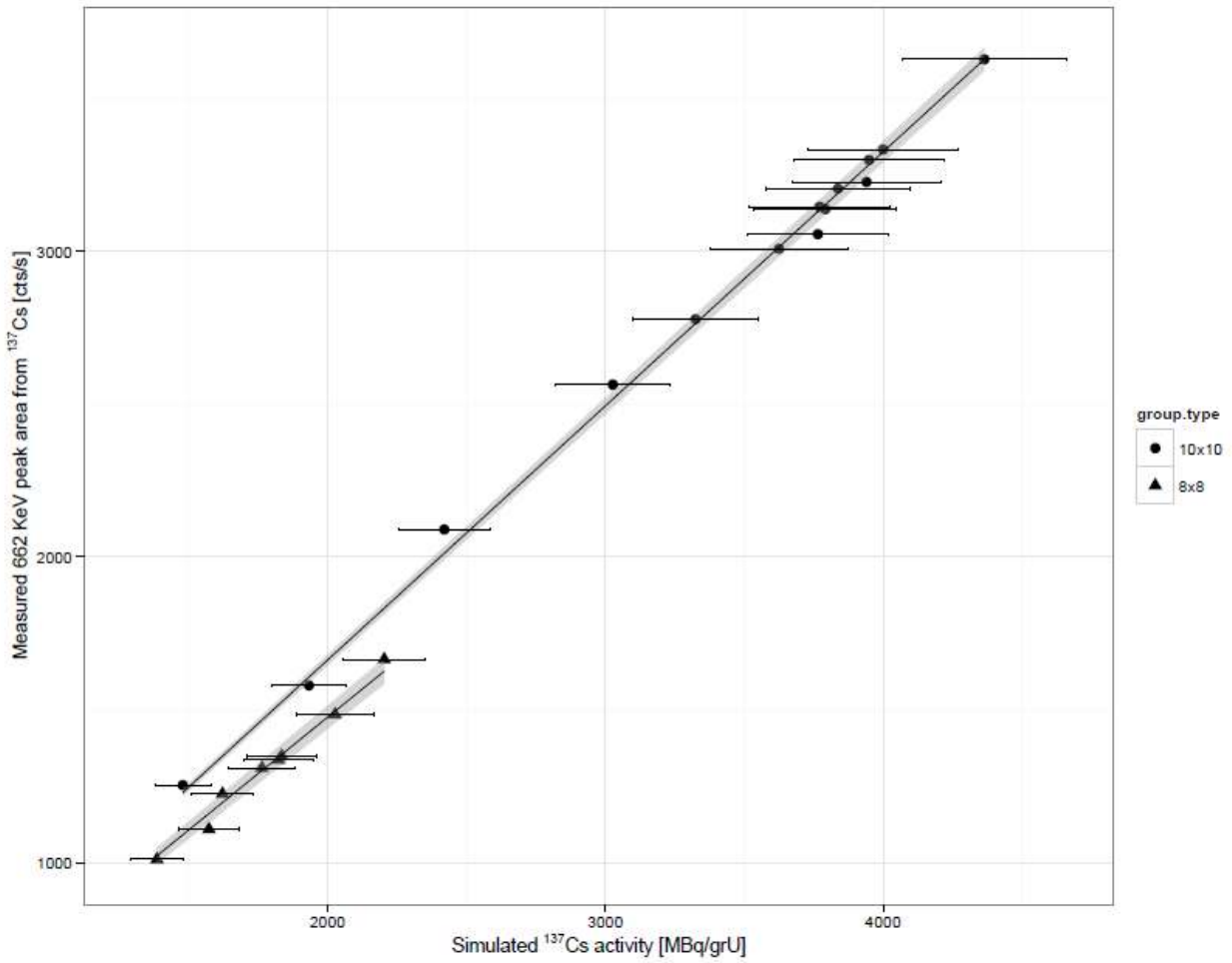

Figure 17. Comparison between the ^{137}Cs measured peak intensity and the corresponding activity calculated by ORIGEN-ARP as normalized by the uranium mass (when not visible, the vertical error bars are smaller than the data points).

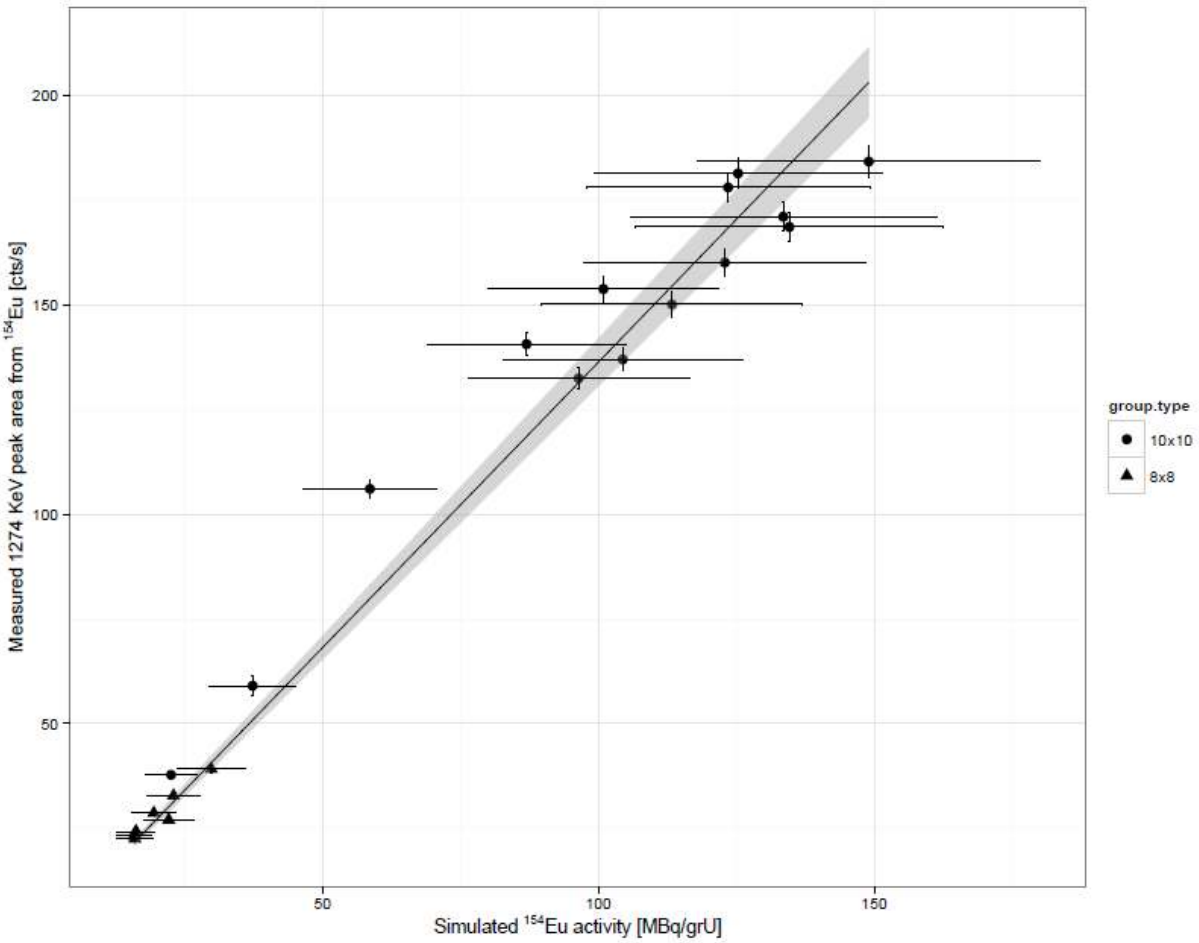

Figure 18. Comparison between the ^{154}Eu measured peak intensity and the corresponding activity calculated by ORIGEN-ARP and normalized by the uranium mass (when not visible, the vertical error bars are smaller than the data points).

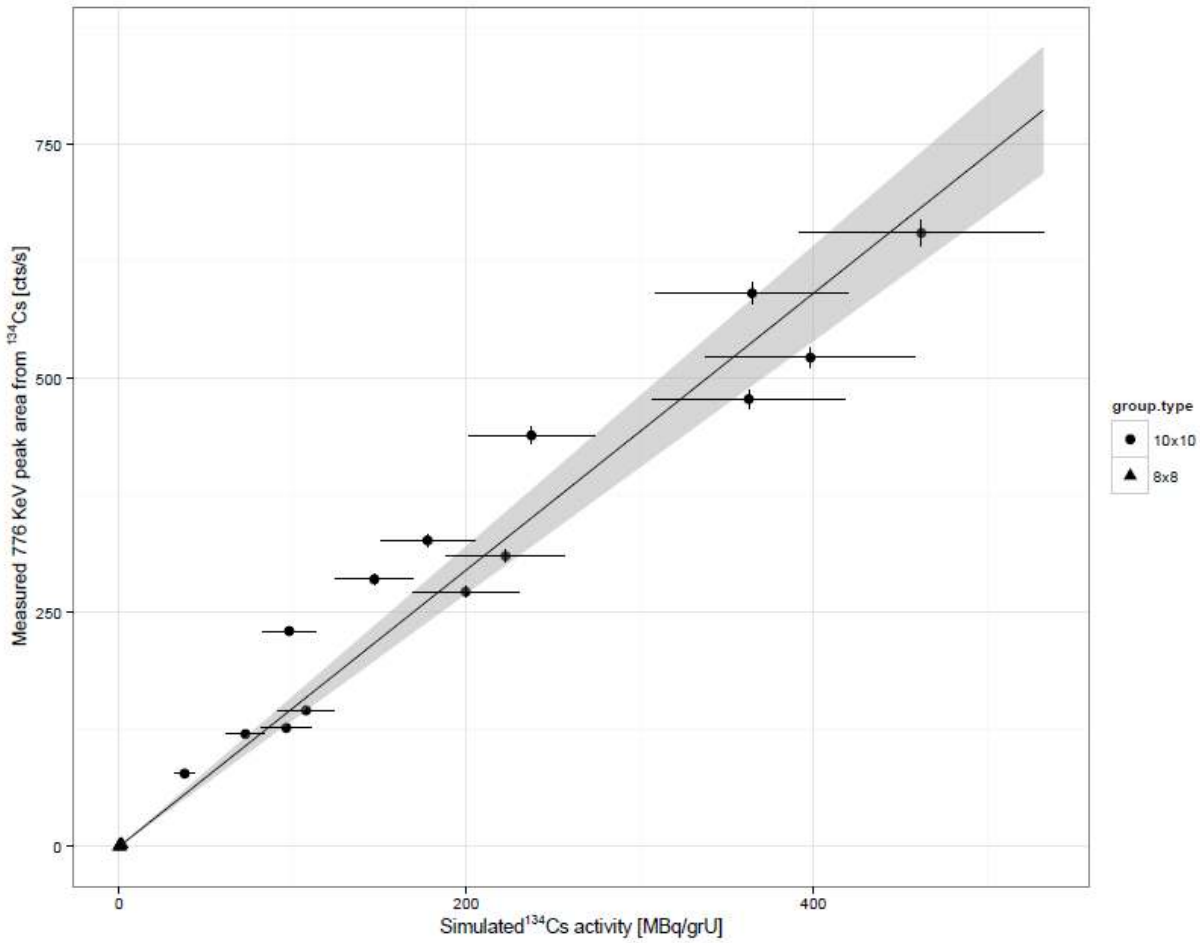

Figure 19. Comparison between the ^{134}Cs measured peak intensity and the corresponding activity calculated by ORIGEN-ARP and normalized by the uranium mass (when not visible, the vertical error bars are smaller than the data points).

The ^{137}Cs plot depicted in Figure 17 is particularly interesting. In fact, a separation between the 8×8 and 10×10 assemblies is evident. Given that the count rate plotted on the vertical axis is derived from the experimental data, all aspects that might cause a separation between the two fuel types are included (mass difference per unit vertical length, irradiation and photon transport effects, etc.). However, for the simulated ^{137}Cs activity on the horizontal axis, only the amount of the ^{137}Cs produced is included. If all relevant physics were included in the simulation, we would anticipate a smooth variation between the measured and the simulated results. Thus, the discontinuity that is observed between the two fuel types is due to neglected physics in the simulation results. In particular, the omission of photon propagation from the fuel to the detector is anticipated to be a large part of the discrepancy. To quantify the count rate

difference due to this fuel type difference, the ratio of the slope of the two curves in Figure 16 was used to form a correction factor. This correction factor adjusts for the fact that a given amount of ^{137}Cs activity in the fuel does not result in the same detected signal in the 662-keV peak for each assembly type. In fact, for the same estimated activity, the 10x10 assemblies produced 12.67% more detected 662-keV gamma rays in the measured peak, as compared with the 8×8 assemblies. Using this correction factor, the measured peak intensity for the 8×8 assemblies in Figure 10 was increased by 12.67%, rendering consistent trending, as compared with the function of burnup among all BWR assemblies, as illustrated in Figure 20.

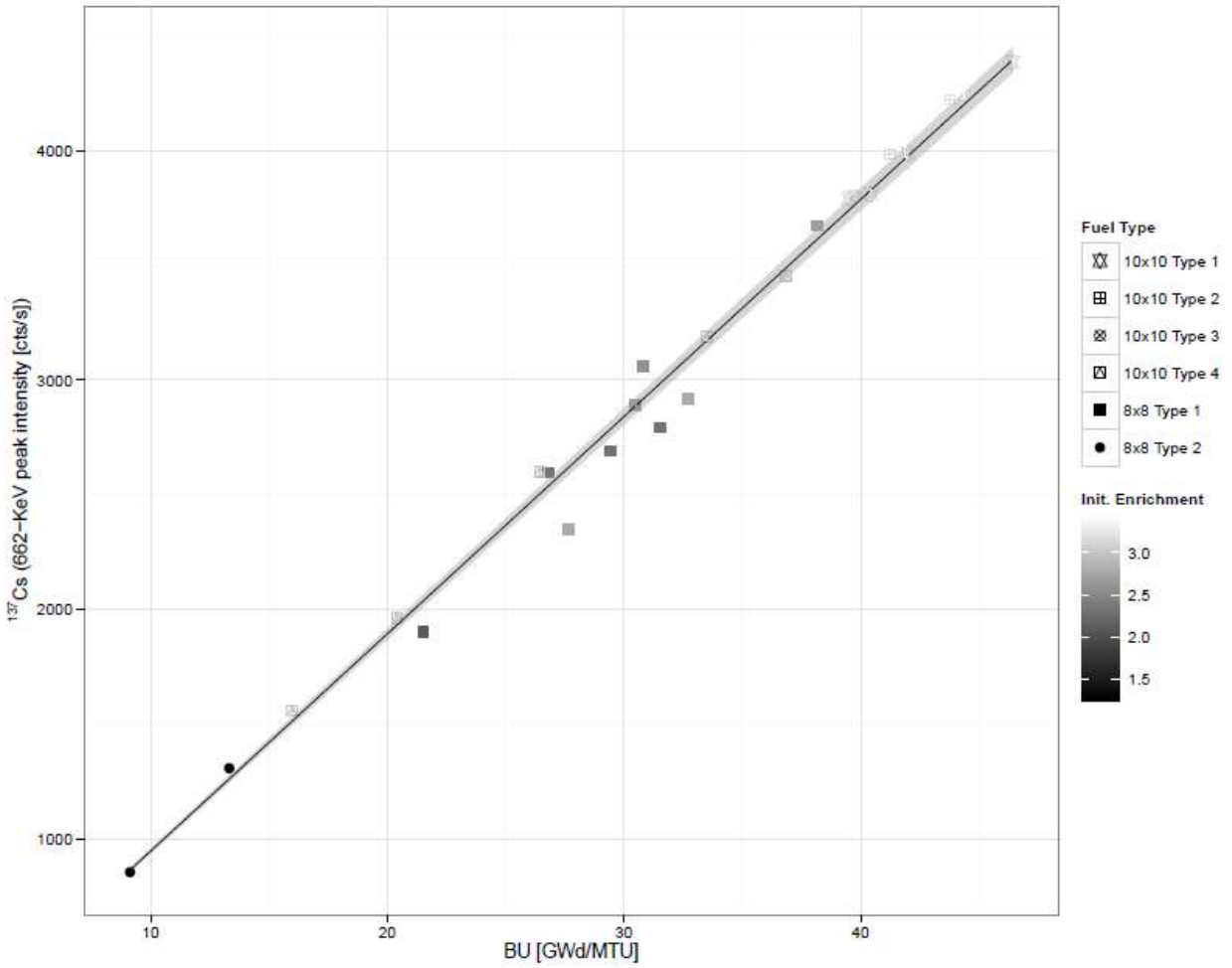

Figure 20. Plot of ^{137}Cs vs burnup for BWR assemblies after applying a correction factor for different self-absorption between the 8×8 and the 10×10 fuel types (when not visible, the error bars are smaller than the data points).

The simulated activity of ^{154}Eu and ^{134}Cs, using only the declared safeguards data, provides general agreement with the measurement spectral data, as illustrated in Figures 17 and 18. These calculations provide a point of comparison for future research that will use the more detailed reactor operator declarations. It is important to quantify the capability of burnup calculations done with both sets of data to understand what is available to inspectorates when only the minimum safeguards-required data are provided or what might be concluded if more detailed data were provided and used.

The lack of a detailed power history as input in the simulations resulted in greater scattering of the data points. In particular, the between-cycles cooling periods were not provided by the nuclear operator, thus were not taken into account in the ORIGEN ARP calculation, with consequent alteration of the resulting shorter-lived nuclides buildup.

Finally, no uncertainty was available on the operator fuel calculation results, used as input for ORIGEN-ARP, so it was impossible to include this variance component in the uncertainty budget. However, an estimate of the uncertainty of ORIGEN calculations is available from validation studies based on comparisons between calculations and destructive analysis [27]: for the ENDF/B-V libraries the 1-sigma estimated variations are 7.6% for ^{134}Cs, 3.7% for ^{137}Cs and 9.8% for ^{154}Eu. In Figures 17, 18 and 19, horizontal error bars represent a 2-sigma variation.

Conclusions

A collaborative research effort among SKB, EURATOM, and the US Department of Energy (DOE) conducted four passive gamma measurement campaigns at the Clab facility in Sweden. The long-term goal of this collaborative team is to demonstrate the merits of different integrated NDA instruments for addressing safeguards and non-safeguards needs as compared with the capability of currently deployed instruments, such as the Fork detector and/or the Digital Cerenkov Viewing Device (DCVD). The current

study fits into this larger context by presenting the summarized results of over 400 spectra obtained from 50 assemblies. Given the complexity of the fuel measured (eight different PWR and six different BWR fuel designs, fuel irradiated at different times over 3 decades, some fuel with burnable poisons and some without, etc.) and categorizing how the measured signatures change (or do not change) with such parameters, it is important to achieve the collaborations' technical goals. For the 25 PWR assemblies, the trends in the spectral signatures of ^{137}Cs, ^{134}Cs, and ^{154}Eu as a function of burnup did not vary in a manner consistent with the number of pins in the assembly (15 × 15 vs 17 × 17), nor did the presence or absence of burnable poisons have a clear impact. For the 25 BWR assemblies, the same trends analysis was undertaken as a function of burnup. In this case, the ^{137}Cs count rate of a 10×10 assembly was measured to be higher than a 8×8 assembly of the same burnup by 12.67%. For both PWR and BWR assemblies, abnormally long periods out of the reactor between initial and final irradiation were evident in the ^{137}Cs data, but not so in the ^{134}Cs and ^{154}Eu signals. ORIGEN-ARP simulations were performed, indicating general agreement when only the safeguards declared data were used. Such comparisons indicate the capability and limitations of such simulations to reproduce the broad trends in the isotopic content from which the spectral signals are produced, especially in relation to the data available to the safeguards inspectorates. Finally, the outcome of the current study consists ultimately of a unique gamma spectroscopic dataset, which in the future can constitute the baseline of a next generation of irradiated fuel verification tools for nuclear safeguards.

Acknowledgments

The authors acknowledge (1) the valued assistance of the operations team at the SKB's Central Interim Storage Facility for Spent Nuclear Fuel (Clab) in Sweden; (2) the Next Generation Safeguards Initiative (NGSI), Office of Nonproliferation and Arms Control (NPAC), National Nuclear Security Administration (NNSA); and (3) Action Sheet 50 under the US DOE-EURATOM cooperation agreement.

References

[1] K.D Veal, S.A. LaMontagne, S.J. Tobin and L.E. Smith, NGSI Program to Investigate Techniques for the Direct Measurement of Plutonium in Spent LWR Fuels by Nondestructive Assay, 51th Annual Miting. of the Institute of Nuclear Material Management, Baltimore, MD July 11-16 (2010).

[2] M.A. Humphrey, S.J. Tobin, and K.D. Veal, The Next Generation Safeguards Initiative's Spent Fuel Nondestructive Assay Project, Journal of Nuclear Material Management, Vol. 40, No.3 (2012).

[3] S.J. Tobin, H.O. Menlove, M.T. Swinhoe, P. Blanc, T. Burr, L.G. Evans, A. Favalli, M.L. Fensin, C.R. Freeman, J. Galloway, J. Gerhart, A. Rajasingam, E. Rauch, N.P. Sandoval, H. Trellue, T.J. Ulrich, J.L. Conlin, S. Croft, J. Hendricks, V. Henzl, D. Henzlova, J.M. Eigenbrodt, W.E. Koehler, D.W. Lee, T.H. Lee, A.M. LeFleur, M.A. Schear, M.A. Humphrey, L. Smith, K.K. Anderson, L.W. Campbell, A. Casella, C. Gesh, M.W. Shaver, A. Misner, S.D. Amber, B.A. Ludewigt, B. Quiter, A. Solodov, W. Charlton, A. Stafford, A.M. LaFleur, C. Romano, J. Cheatham, M. Ehinger, S.J. Thompson, D.L. Chichester, J.L. Sterbent, J. Hu, A. Hunt, W.E. Koehler, V. Mozin, J.G. Richard, and L.E. Smith, "Technical Cross-Cutting Issues for the Next Generation Safeguards Initiative's Spent Fuel Nondestructive Assay Project," *Journal of Nuclear Materials Management* 40(3), pp.18-24, 2012.

[4] IAEA Department of Safeguards Long-Term R&D Plan, 2012-2023, January 2013 (STR-375).

[5] S.J. Tobin, H. Liljenfeldt, H.R. Trellue et al., Experimental and Analytical Plans for the Non-destructive Assay System of the Swedish Encapsulation and Repository Facilities Proceedings of International Atomic Energy Agency Symposium on International Safeguards: Linking Strategy, Implementation and People, Vienna (Austria), 2014, IAEA-CN-220-238.

[6] T.Burr, H.Trellue, S.Tobin, A.Favalli, J.Dowel, V.Henzl, V.Mozin, Integrated Nondestructive Assay Systems to Estimate Plutonium in Spent Fuel Assemblies, Nuclear Science and Engineering, 179, 2015, pages 1-12

[7] C. Willman, A. Håkansson, O. Osifo, A. Bäcklin, S. Jacobsson Svärd., Nondestructive Assay of Spent Nuclear Fuel with Gamma-Ray Spectroscopy, Annals of Nuclear Energy 33:5, pp. 427–438 (2006).

[8] P. Jansson, Studies of Nuclear Fuel by Means of Nuclear Spectroscopic Methods, Ph. D. Thesis, Department of Radiation Sciences, Uppsala University, Uppsala, Sweden (2002). URL(2016-03-18): http://urn.kb.se/resolve?urn=urn:nbn:se:uu:diva-2057

[9] P. Jansson, S. J. Tobin, H. Liljenfeldt, M. L Fugate, A. Favalli, A. Sjöland; Axial and azimuthal gamma scanning of nuclear fuel - implications for spent fuel characterization; Submitted to Journal of Nuclear Materials Management (JNMM); (4 March 2016).

[10] GBS Elektronik GmbH: MCA-527 Multi Channel Analyser, User Manual. http://www.gbs-elektronik.de/fileadmin/_download/manuals/MCA527_Manual_2012_08_07.pdf, last accessed November 3, 2015

[11] T.E. Sampson, T.A. Kelley, and D.T. Vo; Application Guide to Gamma-Ray Isotopic Analysis Using the FRAM Software, Los Alamos National Laboratory report LA-14018 (2003).

[12] D.T. Vo and T.E. Sampson, FRAM, Version 5 User Manual, Los Alamos National Laboratory document LA-UR-11-03005 (2011).

[13] D.T. Vo, A. Favalli, B. Grogan, P. Jansson, H. Liljenfeldt, V. Mozin, P. Schwalbach, A. Sjöland, S.J. Tobin, H. Trellue, S. and Vaccaro, Determination of Initial Enrichment, Burnup, and Cooling time of Pressurized Water Reactor Spent Fuel Assembliess by Analysis of passive Gamma Spectra Measured at the Clab Interim Fule Storage Facility in Sweden, Los Alamos National Laboratory report LA-UR-15-24252 (2015), published in proceedings of the Institute of Nuclear Materials Management (INMM), 56th Annual Meeting , Indian Wells, USA, July 12-16 (2015).

[14] A. Favalli, D.T. Vo, B. Grogan, P. Jansson, H. Liljenfeldt, V. Mozin, P. Schwalbach, A. Sjöland, S.J. Tobin, H. Trellue, S. Vaccaro, Determining Initial Enrichment, Burnup And Cooling Time Of Pressurized-Water-Reactor Spent Fuel Assemblies By Analyzing Passive Gamma Spectra Measured At The CLAB Interim-Fuel Storage Facility In Sweden, NIM-A, 820, 1 June 2016, Pages 102-111

[15] D.T. Vo A. Favalli, B. Grogan, P. Jansson, H. Liljenfeldt, V. Mozin, P. Schwalbach, A. Sjöland, S.J. Tobin, H. Trellue, S. Vaccaro, S., Passive Gamma Analysis of the Boiling-Water-Reactor Assemblies, NIM-A,Volume 830, 11 September 2016, Pages 325–337 (2016) .

[16] Canberra Industries, Genie 2000 Spectroscopy Software—Operations Manual (2006).

[17] B. D. Rooney, PeakEasy Software. Version 1.01. Los Alamos National Laboratory software LA-CC-0028, 2006.

[18] R. Berndt, P. Mortreau, JRC scientific report, Performance test of the Multi-Channel Analyzer MCA-527 for Nuclear Safeguards Applications Test in the PERLA Laboratory at JRC, Ispra, Official European Commission Publication EUR 26165, ISBN 978-92-79-33197-8.

[19] J.M. Chambers, Statistical Models in S, Chapter 4, eds J. M. Chambers and T. J. Hastie, Wadsworth & Brooks/Cole (1992).

[20] J. Maindonald, W. J. Braun, Data Analysis and Graphics Using R, Chapter 5, Cambridge Series in Statistical and Probabilistic Mathematics, Cambridge University Press (2007).

[21] SCALE: A Modular Code System for Performing Standardized Computer Analyses for Licensing Evaluations, ORNL/TM-2005/39, Version 6, Vols. I–III, January 2009. Available from Radiation Safety Information Computational Center at Oak Ridge National Laboratory as CCC-750.

[22] S. Jacobsson, A. Håkansson, C. Andersson, P. Jansson and A. Bäcklin, A tomographic Method for Verification of the Integrity of Spent Nuclear Fuel, Uppsala University SKI report, 98:17 (1998). http://urn.kb.se/resolve?urn=urn:nbn:se:uu:diva-187217 (last accessed Jan.20th,2016).

[23] R. Berndt, Verification of Spent PWR Fuel Data using the ^{154}Eu, ^{134}Cs and ^{137}Cs Activities, Kernenergie (Berlin); v. 31(2) p. 59-63 (1988).

[24] 2012 World Nuclear Industry Handbook, Nuclear Engineering International, http://viewer.zmags.com/publication/95b5bc6a#/95b5bc6a/237. (last accessed Jan.20th,2016)

[25] J. Hu, I.C. Gauld, J. Banfield, and S. Skutnik, Developing Spent Fuel Assembly Standards for Advanced NDA Instrument Calibration – NGSI Spent Fuel Project, technical report ORNL/TM-2013/576, Oak Ridge National Laboratory, Oak Ridge, TN, USA (2014).

[26] Canberra Lynx® Digital Signal Analyzer datasheet, http://www.canberra.com/products/radiochemistry_lab/pdf/Lynx-SS-C38658.pdf, last accessed on November 3, 2015.

[27] G. Ilas, I. C. Gauld, G. Radulescu “Validation of new depletion capabilities and ENDF/B-VII data libraries in SCALE”, Annals of Nuclear Energy 46 (2012) 43–55